Sec and Tat mediated secretion safeguards *Mycobacterium tuberculosis* membrane homeostasis

Priyadarshini Sanyal[1,2,#], Jagadeeshwari Uppada[1,#], Shashank Sinha[4], Yashasvi Bhat[1], Sidra Khan[3,9], Shri Vishalini Rajaram[4,5], Evanjalee Albert Arokiyaraj[4,5], Gagan Deep Jhingan[3,6], Nisheeth Agarwal[7], Areejit Samal[4,8*] and Vinay Kumar Nandicoori[1,2,3*]

1. CSIR-Centre for Cellular and Molecular Biology (CSIR-CCMB), Hyderabad, Telangana, 500007, India
2. Academy of Scientific and Innovative Research (AcSIR), Ghaziabad, Uttar Pradesh, 201002, India
3. BRIC-National Institute of Immunology (BRIC-NII), New Delhi, 110067, India
4. The Institute of Mathematical Sciences (IMSc), Chennai, Tamil Nadu, 600113, India
5. Center for Biotechnology, Anna University, Chennai, Tamil Nadu, 600025, India
6. Current affiliation: Valerian Chem Private Limited, Noida, Uttar Pradesh, 201301, India
7. BRIC-Translational Health Science and Technology Institute (BRIC-THSTI), Faridabad, Haryana, 121001, India
8. Homi Bhabha National Institute (HBNI), Mumbai, Maharashtra, 400094, India
9. Current affiliation: Department of Microbiology, Immunology, and Cancer Biology, University of Virginia, Charlottesville, Virginia, United States of America

* Address correspondence to: vinaykn@nii.ac.in or vinaykn.ccmb@csir.res.in & asamal@imsc.res.in

[#] Both the authors contributed equally

Abstract

Protein secretion drives *Mycobacterium tuberculosis* (*Mtb*) physiology and pathogenesis, yet a unified picture of the machinery and its role in cell membrane homeostasis is still lacking. By comprehensively curating published evidence, we assembled a systems-level map of *Mtb* secretion encompassing 92 components and 198 mechanistic reactions across Sec, Tat, and ESX pathways. The secretory components identified were integrated with high-throughput ChIP-Seq and transcriptome datasets to elucidate the regulation of the secretion system. Using CRISPRi, conditional depletion of SecA1 or TatA impaired growth *in vitro* and survival *ex vivo*. Quantitative secretome revealed decreased export of SecA1- and TatA-dependent substrates, with enrichment of cytosolic proteins in culture filtrates, indicating increased membrane permeability. Membrane proteomics showed depletion dependent increased metabolic/lipid-degrading proteins and decreased cell-wall/cell-process proteins, consistent with loss of membrane stability. Ultrastructural defects and increased ethidium bromide uptake confirmed impaired membrane integrity. Together, our multi-omics and functional genetics established SecA1 and TatA as essential guardians of *Mtb* membrane integrity which provided valuable datasets and a framework for secretion-dependent *Mtb* pathogenesis.

Keywords

Protein secretion, secretory components, CRISPRi knockdown, secretome, membrane proteome, membrane permeability

46 Introductions

47 Protein secretion, a ubiquitous mechanism for transporting macromolecules across
48 membranes, is found in all three domains of life: *Prokaryota, Archaea, and Eukaryota*.
49 Eukaryotic protein secretion occurs through a general pathway called "Sec pathway," which
50 is present in the endoplasmic reticulum (ER) membrane and involves secretory vesicles
51 carrying proteins to the Golgi apparatus[1]. In prokaryotes, the proteins are mainly secreted
52 through two pathways, namely the Sec-dependent pathway[2,3], and the Sec-independent, i.e.,
53 the twin-arginine translocation pathway (Tat pathway)[4], which is also conserved in plants[5].
54 Sec or Tat pathways primarily translocate proteins from the cytoplasmic space to the
55 periplasmic space, cell envelope, or extracellular milieu[6,7]. Proteins that are secreted through
56 Sec and Tat pathways are identified by their respective N-terminal signal peptides[8].

57 Sec-dependent secretion is divided into two types: a) co-translational translocation
58 (Signal Recognition Particle (SRP)-mediated), which exports unfolded proteins while being
59 translated by ribosomes, and b) post-translational translocation (SecA1 and SecA2-mediated),
60 which exports unfolded proteins post-translation[9]. The Sec secretion system comprises SecY,
61 SecE, and SecG proteins[9-11], which form the SecYEG-SecDF-YajC-YidC holotranslocon, with
62 the help of auxiliary proteins SecD, SecF, YajC, YidC[12]. SRP and SecA recognize the emerging
63 preprotein with an N-terminal Sec-signal peptide. For SRP mediated transport, FtsY acts as a
64 receptor and translocation occurs using GTP hydrolysis, whereas SecA as an ATPase, supplies
65 energy for SecA mediated protein translocation[13]. Type I and II signal peptidases, associated
66 with the holotranslocon, act on the cleavage sites, facilitating the conversion to a mature
67 protein[8,14]. The twin-arginine translocation (Tat)[15] system in prokaryotes and the thylakoid
68 membrane of plant chloroplasts[4] is involved in secreting a subset of folded proteins[15,16]
69 containing two invariant arginine residues (RR motif)[17]. In *E. coli*, five *tat* genes, i.e., *tatABCDE,*
70 have been reported, among them *tatABCD* are present in an operon[18].

71 *Mycobacterium tuberculosis* (*Mtb*) secretes an array of proteins, including virulence
72 factors, with the help of generalized and specialized secretion pathways. In *Mtb*, the canonical
73 SecA has two paralogs, SecA1 and SecA2[19,20]. While both SecA paralogs have ATPase activity,
74 the non-canonical SecA2 differs from SecA1 in that it only secretes a small set of proteins to

75 the extracellular space, which are known to be involved in virulence[21-24]. The *Mtb* genome
76 does not encode *tatE*, and *tatD* is not involved in Tat-mediated protein export[18]. TatB and
77 TatC form a Tat Complex-I (TC-I) in the inner membrane, and during translocation, bind to
78 TatA to form Tat Complex-II (TC-II), which results in the formation of an oligomeric pore
79 across the membrane that assists in protein translocation in the presence of proton motive
80 force (PMF)[25]. Specialized secretion systems, such as the ESX secretion systems also known as
81 Type VII Secretion systems (T7SS), transport small proteins with PE/PPE, WXG or YXXXD/E
82 motifs[26]. T7SS consists of 5 systems, ESX-1 to ESX-5, which play an essential role in virulence,
83 pathogenesis, iron, zinc homeostasis, and modulation of host-cellular processes[27]. Although
84 each system has its own specific substrates and functions, they share essential structural
85 features and a common evolutionary origin[28]. The widely studied ESX-1 system works in
86 conjunction with ESX-3 and ESX-5. ESX-2 and ESX-4 are less characterized and are known to
87 play important roles in DNA regulation[28] and extracellular heme acquisition[29].
88 There are several gaps in our understanding of this complex network of secretion
89 systems in *Mtb* that we aimed to address. We asked: (i) what are the core and accessory
90 components in different secretion systems, and how are they organized? (ii) How are these
91 components involved in and regulated at multiple stages of protein transport? (iii) What is
92 the role of SecA1 and Tat secretion systems in cell growth and survival, and what are their
93 substrates? (iv) What is the impact of depleting SecA1 and TatA on *Mtb* membrane
94 homeostasis? In this study, we employed a reconstruction approach to integrate molecular
95 components with mechanistic interactions and developed a visual framework encapsulating
96 the secretion process at the systems level. We generated conditional depletion strains of
97 SecA1 and TatAC to explore their biological roles. Proteome analysis of wild-type and
98 depleted strains suggested that, although the secretion of target substrates is compromised,
99 it led to unusual secretion of cytosolic proteins. Experiments suggest that depletion of these
100 systems impacts membrane homeostasis, reflected in changes in morphology and
101 permeability.

102 ## Results

103 ### Reconstruction of Protein Secretion Systems in *Mtb*

104 The reconstruction of the secretory systems in *Mtb* was conducted as depicted in Fig.
105 1a-b. This comprehensive analysis inspired by the work Feizi *et al.* on genome-scale
106 reconstruction of protein secretion system in yeast *Saccharomyces cerevisiae* aimed to
107 elucidate context-specific regulation and pathway activity, providing insights into the
108 secretion system's behaviour across different physiological states. First, we performed an
109 extensive and systematic literature review that encompassed research articles, review papers,
110 and relevant book chapters on bacterial secretory pathways, with a focus on *Mtb*-specific
111 literature. The evidence from the literature was further curated through a systematic query in
112 the MycoBrowser database[30]. The final annotation is based on experimental evidence from
113 either *Mtb* or other bacterial systems, computational predictions that include sequence
114 similarity and domain architecture, and functional studies. This process resulted in a curated
115 list of 92 key secretory components belonging to three different subsystems: Sec dependent
116 (SRP mediated, SecA2 and SecA1 mediated), Sec independent (Tat), and T7SS (Table S1a).
117 Among these, 19 components were unique to Sec pathways, 3 to Tat, and 67 to T7SS,
118 respectively. Four components, namely LepB (Rv2903c), Lgt (Rv1614), LspA (Rv1539), and
119 Ppm1 (Rv2051c), were shared between the Sec and Tat pathways and are primarily involved
120 in the lipidation process and signal peptide cleavage. In contrast, five components, which are
121 primarily chaperones (Rv3417c- GroEL1, Rv0440- GroEL2, Rv3418c- GroES, Rv0009- PpiA, and
122 Rv2582- PpiB), were shared between the Tat and T7SS pathways (Fig. 1b). The structural and
123 functional annotations of the components, including essentiality, subcellular localization,
124 structural features, and biological functions, are listed in Table S1b, along with relevant
125 evidences. The *in silico* predictions of the H37Rv proteome for secretory specific signal
126 sequences resulted in 8 different categories of proteins belonging to Sec and Tat pathways
127 (Fig. 1c). The proteins were categorized into different pathways depending on the presence
128 of Sec/Tat specific signal peptide, lipo motif (LM) and transmembrane domain (TMD).

129 The export mechanism for each protein category, based on the predictions and
130 associated secretory components, was used to frame 198 mechanistic reactions that

131 significantly represent the protein export process in *Mtb* (Table S2a and S2b). These 198
132 mechanistic reactions illustrate the step-by-step procedure involved in protein export, which
133 was utilized to generate a predictive model of secretion systems in *Mtb* (Fig. 2 & Fig. S1-2).
134 The three significant steps involved in protein export are the recognition of the N-terminal
135 signal peptide in the nascent protein, the export of the protein through the respective
136 translocon based on the signal sequences, and finally, the cleavage of the signal peptide,
137 converting it into the mature protein. During translation, a nascent polypeptide with a
138 hydrophobic signal sequence emerges from the ribosome. The SRP complex (Ffh bound to
139 4.5S RNA) recognizes and binds to the signal sequence and the ribosome-nascent chain
140 complex (RNC). This binding temporarily halts translation to prevent improper folding. The
141 SRP-RNC complex is then targeted to the membrane-bound SRP receptor, FtsY. Upon GTP
142 binding and hydrolysis by Ffh and FtsY, the complex is transferred to the SecYEG translocon
143 embedded in the plasma membrane. Translation resumes, and the growing polypeptide is
144 inserted into or translocated across the membrane. Finally, SRP and FtsY dissociate and are
145 recycled for subsequent targeting events (Fig. S2a-d).

146 If a protein lacks an SRP-recognizable signal sequence, it typically follows alternative
147 post-translational pathways for membrane targeting or secretion. One primary route is the
148 SecA1-dependent pathway, where the fully synthesized protein, bound to the trigger factor
149 (ribosomal chaperone), is recognized in the cytoplasm by SecA1, often with the help of
150 chaperones like DnaK/DnaJ or SecB-like proteins that maintain the protein in an unfolded
151 state. SecA1 then delivers the protein to the SecYEG translocon in the membrane and uses
152 ATP hydrolysis to translocate it across (Fig. 2a). Alternatively, proteins with a twin-arginine
153 motif are transported in a folded state via the TAT (Twin-Arginine Translocation) pathway (Fig.
154 2b). The twin-arginine motif (RR-motif) is recognized by TatC present in the complex with
155 TatB and the translocation happens from the pore formed by TatA oligomerization in the
156 inner membrane with the help of proton motive force.

157 The fate and localization of proteins depend on the presence of TMD or LM. If a protein
158 contains a TMD, it is embedded into the inner membrane using the membrane insertase
159 (YidC) during translocation (Fig. S1). If the protein does not have an LM, the signal peptidase

160 LepB cleaves the N-terminal signal peptide. For proteins containing a LM, additional steps of
161 lipidation occur in the inner membrane, involving three enzymes: Lgt (Phosphatidylglycerol:
162 prolipoprotein diacylglyceryl transferase), which adds a diacylglycerol to the thiol of the
163 lipobox cysteine located after the signal sequence; LspA (Signal peptidase II), which cleaves
164 the signal peptide, exposing the lipid-modified cysteine at the N-terminus; and Ppm1, which
165 adds a third amide-linked fatty acid, completing triacylation. The mature triacylated
166 lipoprotein is correctly anchored and functional at the outer membrane or retained in the
167 inner membrane, depending on the transmembrane domains (Fig. S1).

168 In the case of *Mtb*, a smaller subset of proteins that lack classical signal peptides or
169 have atypical ones, such as SodA (superoxide dismutase)[21], KatG (catalase-peroxidase)[21],
170 SapM (Acid phosphatase)[22], PknG (Serine/threonine-protein kinase-G)[31], and certain PE/PPE
171 proteins, are transported through SecA2 transport. SecA2 is predominantly cytosolic and
172 exports proteins in conjunction with the chaperone SatS[32]. SecA2 may function by interacting
173 with SecYEG either independently or in cooperation with SecA1[33]. Some evidence suggests
174 that SecA2 may require SecA1 for effective translocation, possibly forming heterodimers or
175 coordinating the sequential export of substrates[34]. SecA2 reactions were not integrated into
176 the model, as there is no clear evidence of how these proteins are transported. Unlike the
177 canonical Sec system, SecA2 substrates often fold fully or partially before export[33,35].

178 In addition to the aforementioned secretion systems, *Mtb* also contains ESX-1 to ESX-
179 5[36] secretion systems that facilitate the transport of virulent proteins across the membrane to
180 an extracellular environment[37,38]. The proteins transported through ESX are known to feature
181 either a PE/PPE motif or a WXG motif at the N-terminal and a YXXXD/E motif at the C-
182 terminal[26]. Studies have demonstrated that components of the ESX systems create a channel
183 in the inner membrane (Fig. 2c), although the mechanism by which the proteins are exported
184 into the extracellular environment remains unclear. However, recent proteogenetic studies
185 conducted by Cronin et al., 2022[39] showed that the substrates of ESX-1 are co-secreted, and
186 the absence of one gene leads to the loss of both secreted complexes, also outlining the
187 order in which these substrates are transported as described in Table S2.

188 **Integration of Omics data with Secretory Components**

189 The transcriptional regulation of secretory components was analyzed by curating and
190 integrating publicly available ChIP-Seq data[40,41] along with the secretory components listed
191 in this study. This integrative analysis revealed that 68 Transcription Factors (TFs) from 28
192 families were directly involved in regulating secretory components. Most of the TFs belonged
193 to the TetR family, followed by the ArsR family. Among the TFs, 50% (34 of 68) were known
194 to regulate more than four secretory components (Fig. 3a). The major TFs involved in this
195 regulation include Rv0081, which belongs to the ArsR family and directly regulates 12
196 components within the Sec pathway (6), Tat pathway (1), and T7SS (5). The second TF that
197 controls most secretory components is *cosR* (*rv0967*), which plays a vital role in copper
198 homeostasis and directly regulates 11 secretory components. Lastly, *trcR* (*rv1033c*), a
199 response regulator of the two-component system TrcRS, directly regulates nine secretion
200 components (Fig. 3b).

201 Among the 21 factors regulating the expression of more than 2 secretory components
202 and fewer than four components, most belong to the TetR and WhiB families and are primarily
203 observed in controlling the T7SS pathway (Fig. 3c). The expression of secretory components
204 is mainly associated with external stimuli. The stress conditions faced by the organisms aid in
205 secreting various proteins. Therefore, we aimed to examine the transcriptional level
206 expression of the secretory components under several stress conditions, including oxidative,
207 nitrosative, SDS, and acidic stress. This can be achieved by integrating the RNA sequencing
208 data[42] with the secretory components data. We looked at the differential expression of
209 secretory components under various stress conditions compared to their expression in cells
210 grown in 7H9 medium (Control). We observed that starvation and SDS stress significantly
211 impacted the expression of these secretory components relative to other stresses. Most of
212 the Sec and Tat components were downregulated under starvation stress, whereas the
213 opposite was true for the T7SS (Fig. 3d).

214 **Compromised bacterial survival upon *secA1* and *tatAC* depletion**

215 T7SS systems in *Mtb* are extensively investigated in relation to other secretion
216 pathways, specifically the Sec and Tat pathways. The deletion of SecA2 and its impact on the

217 secretome has already been reported. Therefore, in this report, we aim to focus on and
218 investigate the SecA1 and Tat secretion pathways; thus, we selected SecA1 and TatA as the
219 candidates. Furthermore, both SecA1 and TatA are known to be regulated by PknB-mediated
220 phosphorylation[43], which makes them intriguing candidates. High-throughput transposon
221 mutagenesis studies indicate that both *secA1* and *tatA* are essential genes for *in vitro* growth
222 in complete media.

223 We generated CRISPRi-mediated knockdown strains[44] of *secA1* and *tatA*. Towards this,
224 either the pTetIntdCas9 vector or the pTetIntdCas9 harboring two guide RNAs (Fig. S3a)
225 targeting *secA1* or *tatA* (Fig. S3b) were electroporated into *Mtb* to create *Rv-vc*$_{dc}$, *Rv-secA1*$_{dc}$,
226 and *Rv-tatA*$_{dc}$ strains. The addition of ATc results in the expression of dCas9 and the guide
227 RNA, along with their handle, which form a complex and stall transcription (Fig. S3c). The
228 depletion of SecA1 and TatA upon the addition of ATc and the expression of the were
229 confirmed by Western blotting with α-SecA1 and α-TatA antibodies, respectively (Fig. 4b).
230 Depletion of either SecA1 or TatA resulted in compromised growth *in vitro* (Fig. 4a).

231 The CRISPRi system is known to cause polarity effects for the entire operon[44]. While
232 *secA1* is a solo gene, *tatA* is the first gene in a two-gene operon that also includes *tatC*. Both
233 *tatA* and *tatC* are essential *in vitro* and are part of the Tat secretion pathway. To evaluate the
234 polarity effect, total RNA was isolated from the *Rv-vc*$_{dc}$, *Rv-secA1*$_{dc}$, and *Rv-tatA*$_{dc}$ strains in
235 the presence and absence of ATc, and the expression levels of *secA1*, *tatA,* and *tatC* were
236 quantified (Fig. 4c). Upon the addition of ATc, although we were targeting only *tatA*, the
237 expression levels of both *tatA* and *tatC* were compromised. Thus, we used *tatA*$_{gmut}$ alongside
238 *tatC* to complement *Rv-tatA*$_{dc}$. We electroporated complementation constructs pSNG-
239 secA1$_{gmut}$ or pSNG-tatAC$_{gmut}$, in which the guide RNA target sequences were mutated (Fig.
240 S3d), into *Rv-secA1*$_{dc}$ and *Rv-tatA*$_{dc}$ strains, respectively, to generate *Rv-secA1*$_{dc}$*::secA1* and
241 *Rv-tatA*$_{dc}$*::tatAC* (Fig. S3e).

242 The functional complementation was validated by enumerating CFU *in vitro* and in *ex*
243 *vivo*. The cells were grown in 7H9 media, and CFUs were enumerated at different time points.
244 In the *Rv-secA1*$_{dc}$ +ATc strain, compromised growth was observed around ~4 $\log_{10}$ fold as
245 compared to *Rv-vc*$_{dc}$ +ATc after 4 days of depletion (Fig. 4d). While in the case of *Rv-tatA*$_{dc}$

246 +ATc, the growth defect was noticed around ~3 $\log_{10}$ fold (Fig. 4d). The growth phenotypes
247 were rescued by complementation. In the peritoneal macrophages (Fig. 4e), the growth was
248 compromised up to ~2.5 $\log_{10}$ fold in *Rv-secA1*$_{dc}$ +ATc and ~0.8 $\log_{10}$ fold in *Rv-tatA*$_{dc}$ +ATc
249 as compared to *Rv-vc*$_{dc}$ +ATc control (Fig. 4f). The complementation strains rescued the
250 growth phenotype. We conclude that we successfully generated the *Rv-secA1*$_{dc}$ and *Rv-tatA*$_{dc}$
251 knockdown strains, indicating that *secA1* and *tatAC* (*tatA* and *tatC*) are essential for bacterial
252 survival.

253 **Change in the secretome upon SecA1 and TatAC depletion**

254 SecA1 and TatAC are important players involved in Sec and Tat-mediated secretion
255 pathways. While *in silico* studies provide predictions on putative Sec or Tat substrates based
256 on the presence of consensus signal peptides or twin arginine motifs, respectively, there are
257 no experimental studies that confirm these predictions. To identify the SecA1- and Tat-
258 mediated secretome, *Rv-vc*$_{dc}$, *Rv-secA1*$_{dc}$, and *Rv-tatA*$_{dc}$ strains were grown to the early log
259 phase (A_{600} ~0.4) in the presence of ATc. Cells were spun down, the pellet was processed for
260 WCL, and the supernatant was enriched for the culture filtrate (CF) proteins[45] (Fig. S4a). The
261 WCL and CF fractions were resolved and probed with α-PknB and α-Ag85B antibodies, which
262 are markers for membrane/WCL and secreted proteins, respectively (Fig. S4b). Absence of
263 band corresponding to PknB and presence of Ag85B bands in CF fractions is indicative of the
264 lack of contamination from other fractions. Ag85B is shown to be secreted through SecA
265 pathway in *E. coli*[46]. As anticipated, we observed that Ag85B levels were lower upon the
266 depletion of SecA1; however, we also observed decreased levels of Ag85B upon TatAC
267 depletion. We cannot rule out the possibility that Ag85B may use more than one secretory
268 pathway for its secretion.

269 The CF fractions in triplicates were trypsinized, and the resulting tryptic peptides were
270 resolved using LC-MS/MS, followed by data analysis with label-free quantitation (LFQ). The
271 data was further processed as outlined in Fig. 5a. A total of 1255 proteins were present in all
272 three samples namely: *Rv-vc*$_{dc}$ +ATc, *Rv-secA1*$_{dc}$ +ATc, and *Rv-tatA*$_{dc}$ +ATc. Proteins with ≤ 2
273 unique peptides or with more than one transmembrane helix were filtered out, which
274 decreased the number to 1010 proteins. This was followed by filtering to remove proteins

275 identified as part of membrane vesicles, which further decreased the number to 932 proteins.
276 The resultant secretome obtained for *Rv-secA1*$_{dc}$ +ATc and *Rv-tatA*$_{dc}$ +ATc was compared
277 with *Rv-vc*$_{dc}$ +ATC to identify the differences. We hypothesized that the absence of SecA1 or
278 TatAC would lead to a substantial decrease in the number of secreted proteins. Contrary to
279 our hypothesis, we observed a higher number of secreted proteins, which included known
280 cytosolic proteins in both *Rv-secA1*$_{dc}$ +ATc and *Rv-tatA*$_{dc}$ +ATc samples, which could be due
281 to changes in overall cellular homeostasis upon depletion (Table S5).

282 Therefore, to accurately analyze the changes in the secretome, we limited our analysis
283 to secretory proteins that were common between the current study and at least one other
284 previously published study (among the four previous studies[47-50]) (Fig. S4d). This reduced the
285 number of secretory proteins selected for further analysis from 932 to 439. We compared *Rv-*
286 *vc*$_{dc}$ +ATC with *Rv-secA1*$_{dc}$ +ATc or *Rv-vc*$_{dc}$ +ATC with *Rv-tatA*$_{dc}$ +ATc samples, and only those
287 with a ±2 fold change were considered for further analysis. We obtained a total of 134
288 proteins that were differentially secreted in *Rv-secA1*$_{dc}$ +ATC, with 66 showing >2 fold higher
289 abundance and 68 showing lower abundance (Fig. 5b). The numbers were 158 differentially
290 secreted proteins, with 81 showing >2 fold higher abundance and 77 showing lower
291 abundance for the *Rv-tatA*$_{dc}$ +ATc samples (Fig. 5c). Applying a p-value cut off <0.05 for the
292 differentially abundant secretory proteins reduced the final counts to 118 (58 with higher and
293 60 proteins with lower abundances) for *Rv-secA1*$_{dc}$ +ATC and 138 (75 proteins with higher
294 abundance and 63 with lower abundance) for *Rv-tatA*$_{dc}$ +ATc samples (Fig. 5d & e). Among
295 these, 72 proteins were common between *Rv-secA1*$_{dc}$ +ATc and *Rv-tatA*$_{dc}$ +ATc samples, with
296 proteins exhibiting similar increased or decreased abundance patterns in both samples (Fig.
297 S4e).

298 We reasoned that the proteins less abundant in *Rv-secA1*$_{dc}$ +ATc but not in *Rv-tatA*$_{dc}$
299 +ATc samples are specific substrates of the SecA1 pathway (Fig. 4Sd-27 proteins), and those
300 less abundant in *Rv-tatA*$_{dc}$ +ATc but not in *Rv-secA1*$_{dc}$ +ATc are specific Tat pathway
301 substrates (Fig. 4Sd-30 proteins). The remaining 33 less abundant proteins (Fig. 4Sd-33
302 proteins) are either substrates of both pathways or require components from both pathways
303 for efficient secretion. Among the 27 unique substrates of the SecA1 pathway, 13 proteins

304 had SecA1 signal peptide (SP) and SP + LM (Fig. 5f). Among the 30 unique substrates of the
305 Tat pathway, only 5 proteins were found to have a predicted Tat signal and Tat signal + LM.
306 These results indicate that many of the less abundant proteins identified in the current study
307 are not predicted to be substrates of these pathways, which may require further validation.

308 We also observed that a total of 58 and 75 secretory proteins were highly abundant
309 (>2 fold and p-value <0.05) in *Rv-secA1*$_{dc}$ +ATc and *Rv-tatA*$_{dc}$ +ATc (Fig. 5d-e; Table S5).
310 Among these, 39 proteins were common to both samples, while 19 were unique to *Rv-secA1*$_{dc}$
311 +ATc and 36 were unique to *Rv-tatA*$_{dc}$ +ATc. Of the 58 abundant proteins in *Rv-secA1*$_{dc}$ +ATc,
312 57 did not possess any N-terminal signal peptides. Proteins predicted to be secreted via T7SS
313 and SecA2 pathways were highly abundant in *Rv-tatA*$_{dc}$ +ATc. We speculate that the higher
314 abundance of proteins in *Rv-secA1*$_{dc}$ +ATc and *Rv-tatA*$_{dc}$ +ATc samples could be due to
315 increased non-classical secretion (T7SS or SecA2). Furthermore, there is a possibility that
316 depletion of the SecA1 and TatAC, known to be associated with the export of proteins
317 involved in membrane stabilization, could have compromised the *Mtb* membrane integrity,
318 leading to leakage of periplasmic or cytoplasmic proteins into the CF fraction. To address this,
319 we investigated the changes in the membrane proteome upon SecA1 and TatAC depletion.

320 **Mycobacterial membrane proteome alteration owing to SecA1 and TatAC depletion**

321 Next, we examined the protein composition of membrane fractions from *Rv-vc*$_{dc}$ +ATc,
322 *Rv-secA1*$_{dc}$ +ATc, and *Rv-tatA*$_{dc}$ +ATc samples. The cytosolic and membrane fractions were
323 probed with α-rpoA (a marker for the cytosolic fraction) and α-PknB (a marker for the
324 membrane fraction) antibodies, respectively. The presence of PknB band and RpoA band in
325 the WCL fraction, but not in cytosolic or membrane fractions, respectively, in *Rv-vc*$_{dc}$ +ATc
326 samples suggests the purity of the respective fractions and validates the protocol used. While
327 the fraction of *Rv-tatA*$_{dc}$ +ATc showed a profile similar to *Rv-vc*$_{dc}$ +ATc, we observed the
328 presence of the cytosolic marker in *Rv-secA1*$_{dc}$ +ATc in the membrane fraction (Fig. S5b). The
329 fractions were probed with other cytosolic markers, which supported the above observations
330 (data not shown).

331 The membrane fractions in triplicate were trypsinized, and the samples were resolved
332 by LC-MS/MS, with data processed through label-free quantitation (LFQ) and analyzed as

333 described in Fig. 6a. A total of 2335 proteins were detected in the membrane fractions *of Rv-*
334 *vc$_{dc}$* +ATc, *Rv-secA1$_{dc}$* +ATc, and *Rv-tatA$_{dc}$* +ATc samples. Proteins with ≤2 unique peptides
335 and lacking transmembrane helices were eliminated from 2335 proteins, reducing the number
336 of proteins to 1101. We compared the data obtained from the current study with two
337 previously published membrane proteome studies and identified 943 proteins that were
338 common to two studies[22,51] including our study. We analyzed the abundances of these
339 proteins in *Rv-secA1$_{dc}$* +ATc and *Rv-tatA$_{dc}$* +ATc samples in comparison with *Rv-vc$_{dc}$* +ATc,
340 and the proteins with a ±2 fold change, and with a p-value cut off of <0.05 were considered
341 for further analysis.

342 We observed a total of 260 proteins that were differentially abundant in *Rv-secA1$_{dc}$*
343 +ATc, with 138 and 122 proteins showing high and low abundance, respectively (Fig. 6b & d).
344 The number of differentially abundant proteins identified in *Rv-tatA$_{dc}$* +ATc was much lower,
345 accounting for 81 in total, with 31 being highly abundant and 50 low in abundance (Fig. 6c &
346 e). The results seem to reflect the data observed in western blot (Fig. S5b), where cytosolic
347 markers were detected in *Rv-secA1$_{dc}$* +ATc samples, unlike in *Rv-tatA$_{dc}$* +ATc. A total of 32
348 differentially abundant proteins were common in *Rv-secA1$_{dc}$* +ATc and *Rv-tatA$_{dc}$* +ATc
349 samples. In *Rv-secA1$_{dc}$* +ATc, 19 were high and 13 were low in abundance, while, 15 proteins
350 were high and 17 were low abundant in case of *Rv-tatA$_{dc}$* + ATc (Table 6). Among these 32
351 proteins, Phenolpthiocerol synthesis type-I polyketide synthase (PpsE), Proteasome beta
352 subunit (PrcB), Rv0455c, and Rv1896c, were highly abundant in *Rv-secA1*$_{dc}$ +ATc, whereas
353 they were low in *Rv-tatA*$_{dc}$ +ATc (Table 6). Annotation of differentially abundant proteins
354 based on their functions showed that proteins belonging to cell wall and cell processes were
355 low in abundance in the membrane fraction, while those involved in metabolic processes were
356 more abundant in *Rv-secA1$_{dc}$* +ATc (Fig. 6f). However, both cell wall and cell process proteins,
357 along with metabolic process proteins, were low in abundance in *Rv-tatA$_{dc}$* +ATc (Fig. 6g).
358 Together, the data suggests that there may be a possible membrane dysbiosis in *Rv-secA1$_{dc}$*
359 +ATc samples, which may also be the case with *Rv-tatA$_{dc}$* +ATc, but at a lower scale.
360

361 **SecA1 and TatAC depletion results in Mycobacterial membrane permeability**

362 Data presented in Fig. 5 and 6 showed significant changes in the secretome and
363 membrane proteome upon SecA1 and TatAC depletion. Interestingly, we observed many
364 cytosolic proteins in both the secretome and membrane proteome when compared with Rv.
365 Furthermore, we also observed that many proteins were common to both pathways, which
366 are thought to be distinct. Thus, we speculated that the depletion of SecA1 to a large extent
367 and TatAC to a lesser extent may be compromising the membrane, which could have led to
368 the similarity. To investigate the phenotypic impact of SecA1 and TatAC depletion on cellular
369 morphology, we performed scanning electron microscopy (SEM). We observed bulged and
370 elongated cells (>40% cells were >3μm) upon depletion of SecA1, which could be restored
371 through complementation (Fig. 7a-b & Fig. S6a). While the cells were elongated (>10% cells
372 were >4μm) compared with Rv upon TatAC depletion, which could be complemented, they
373 did not exhibit the bulged phenotype observed upon SecA1 depletion (Fig. 7a-b & Fig. S6a-
374 b). To further investigate the effect of SecA1 and TatAC depletion on the ultrastructure of the
375 *Mtb* membrane, we performed transmission electron microscopy (TEM). We observed that
376 the architecture of the cell membrane was significantly altered upon SecA1 or TatAC
377 depletion and could be restored upon complementation (Fig. 7c). However, we could not
378 observe perforations in the membrane, suggesting that the possible changes at the given
379 time point in the experiment may be more subtle and possibly more permeable.

380 To investigate the changes in the permeability of the membrane, we performed
381 Ethidium Bromide (EtBr) and Propidium Iodide (PI) uptake experiments. If the cells have
382 indeed become more permeable after SecA1 and TatAC depletion, we would expect increased
383 EtBr uptake and a shift in the PI fluorescence intensity compared with $Rv\text{-}vc_{dc}$ +ATC. In line
384 with this hypothesis, we observed increased intensity of EtBr in the cells upon depletion of
385 SecA1 or TatAC for 4 days compared with the control and the 2 days depleted samples (Fig.
386 S6c & d). The increased uptake of EtBr four days post depletion in SecA1 and TatAC depleted
387 samples could be restored to *Rv* levels upon complementation (Fig. S6c & d). For the PI
388 uptake assay, the samples were sorted for the population containing the PI signal using a
389 FACS machine. The results obtained were analogous to those observed in the EtBr uptake

390 assay, with both SecA1 and TatAC-depleted samples showing a shift in fluorescence
391 compared to the undepleted, control, and complemented samples (Fig. 7d). Taken together,
392 depletion of SecA1 or TatAC causes changes in the *Mtb* membrane ultrastructure, which in
393 turn leads to increased permeability.

394 ## Discussion

395 The manual reconstruction of secretion systems in *Mtb*, encompassing 92 secretory
396 components and 198 mechanistic reactions, organizes diverse information on molecular
397 components, which are often scattered as experimental evidence, and the associated
398 mechanistic interactions involved in the secretion process into a systems-level model. The
399 first genome-scale model for protein secretion was developed for yeast, *Saccharomyces*
400 *cerevisiae,* using a bottom-up approach with the Protein Specific Information Matrix (PSIM)
401 framework, providing a systems-level understanding of secretion machinery in eukaryotes[52].
402 Subsequent studies have performed a genome-scale analysis of protein secretion system in
403 *Aspergillus oryzae*[53] and humans[54]. Notably, a later study[55] has integrated the core secretory
404 pathway into genome-scale metabolic models for humans (RECON2.2s), mice (iMM1685s),
405 and CHO cells (iCHO2048s) to determine the energetic costs and machinery demands for
406 secreted proteins. In contrast, most available genome-scale models for prokaryotes mainly
407 focus on metabolic pathways and lack detailed representations of protein secretion
408 machineries and their regulation[56-58]. *Mtb* has been extensively studied with models such as
409 iNJ661[59], GSMN-TB[60], iEK1011[61], and sMtb2018[62], which combine genomic and biochemical
410 data to simulate *Mtb* metabolism under various conditions. However, the available metabolic
411 models for *Mtb* have not been extended to build an integrative model with detailed
412 mechanistic description of protein secretion machinery at the systems-level.

413 *Mtb* relies on Sec, Tat, and multiple specialized secretion systems, such as the Type VII
414 secretion system (T7SS), which includes five ESX systems (ESX-1 to ESX-5) and SecA2. While
415 reports offer detailed mechanistic insights, the modular organization of T7SS[64] and the
416 characterization of SecA2[21] are available independently; however, a single, integrated
417 reconstruction of *Mtb* secretion pathways has not been established. In this study, we aimed
418 to identify all components of secretory systems and to delineate the roles of specific elements
419 (such as SecA1 and Tat) in *Mtb* virulence. Fig. 1 offers a mechanistic characterization of
420 common components in secretion systems, considering the functional evidence from existing
421 experimental data. Instead of relying on computational simulations, we provided a pictorial
422 and conceptual reconstruction that helps visualise the elements of the secretory machinery

423 and their architecture (Fig. 2). The Sec pathway driven by SRP, SecA1 ATPase, and Tat pathway
424 is depicted in our model in detail (Fig. 2 and Fig. S1). By integrating transcriptomic and ChIP-
425 Seq datasets, we identified key transcription factors that regulate the expression of secretion
426 system genes (Fig. 3b), revealing the dynamic regulatory networks that underpin their
427 function, which was absent in most previous studies[35,64,65]. In the future, our reconstruction of
428 *Mtb* secretion systems can be expanded to create a proteome-constrained, genome-scale
429 protein secretory model for *Mtb*, similar to the recently developed model for yeast[66].

430 CRISPRi-mediated knockdown can affect genes downstream of the target gene in an
431 operon. While *secA1* is a single-gene operon, the *tatC* gene is downstream of *tatA* gene. Our
432 qRT-PCR experiments showed that the expression of both *tatA* and *tatC* was downregulated
433 upon induction of guide RNA and dCas9 (Fig. 4). Since both TatA and TatC function in the
434 same secretion pathway, we did not attempt to create a specific TatA depletion strain by
435 complementing with *tatC* at another integrative locus. Multiple groups, including ours, have
436 performed mass spectrometric analysis of the mycobacterial secretome. The number of
437 secretory proteins identified in several major studies ranged from 257[47], 254[48], 481[50] to 932
438 in the current study. The increased numbers in the current study may be due to technical
439 improvements in the mass spectrometer's sensitivity. Here, we focused on 439 proteins that
440 were common between the current study and one of the three previous studies (Fig. 5). A
441 prior study in *Mycobacterium marinum* and *M. marinum esx-5* null identified 30 proteins,
442 including 24 PE/PPE proteins that depended on the presence of ESX-5[67]. Another study
443 identified a total of 66 proteins (33 increased and 33 decreased) that were either became
444 more or less abundant in the *ΔsecA2* mutant compared with the wild type[22]. Here, we report
445 for the first time that secretion of 118 proteins was dependent on SecA1 and 138 on TatAC
446 systems, respectively (Fig. 5). Interestingly, 72 proteins were commonly impacted by both
447 SecA1 and TatAC depletion (Fig. S4), suggesting either dependence on both pathways due to
448 cross-talk or depletion-dependent perturbations in the cell.

449 Upon SecA1 depletion, lipoproteins, which are typically localized to the membrane and
450 contain classical Sec signal peptides, were found to be reduced in abundance (Fig. 5). We also
451 identified RipA, PG endopeptidase[68], and Ami1, an amidase[69] necessary for maintaining PG

452 synthesis, as being lower in abundance (Fig. 5). In *Streptomyces coelicolor*, the authors
453 identified 43 Tat pathway substrates, 25 of which were validated using a sensitive agarase
454 reporter assay[70]. *Mtb* utilizes the Tat pathway to export various proteins, including enzymes,
455 hydrolases, and proteins involved in cell wall processes[17]. Tat-deficient mutants in *Msm* failed
456 to export β-lactamases such as BlaS to the cell envelope, resulting in sensitivity to β-lactam
457 antibiotics[71]. Rv2525c also plays a role in maintaining cell wall integrity and stress adaptation
458 in *Mtb*[72]. We observed lower abundances of Rv2525c and plcB proteins in the Tat-depleted
459 secretome.

460 A total of 528[73], 1417[74], 1318[22], and 1539[51] membrane proteins were obtained from
461 membrane proteome studies conducted by various groups previously, and 2335 were
462 identified in our current study. The variation in the number of membrane proteins may be
463 due to the type of membrane fractionation methods and biological conditions used.
464 Comparing our study with the previous two studies[22,51] resulted in 943 proteins that were
465 common to our study and one of the other two studies. Among these, 260 were differentially
466 abundant in SecA1, and 81 for TatAC depletion (Fig. 6). A previous study showed that 13 out
467 of 15 solute binding proteins (SBPs), 12 out of 21 Mce transporter family members were
468 reduced, and 13 out of 21 identified DosR-regulated proteins were increased in the *ΔsecA2*
469 mutant[22]. Here, we observed that, upon SecA1 depletion, metabolic proteins, mostly those
470 involved in lipid degradation, were highly abundant, while cell wall synthesis proteins were
471 less abundant (Fig. 6). A similar trend was observed in TatAC depletion. A previous study
472 validated the localization of LpqH, a membrane-anchored lipoprotein[75], which was lower in
473 abundance in the membrane fraction upon SecA1 depletion in our study (Fig. S5c).

474 A notable point was that we observed many cytosolic proteins in the secretome upon
475 SecA1 or TatAC depletion, which were not analyzed further because they were not part of the
476 secretome in earlier studies (Fig. S4d & e). We have observed a similar trend even in the
477 membrane proteome upon SecA1 and TatAC depletion (Fig. S5c & d). This observation led
478 to an examination of the ultra-structures by SEM and TEM (Fig. 7). Data Fig. 5-7 suggests that
479 the loss of SecA1 and TatAC appears to disrupt cellular homeostasis, which in turn seems
480 impact the membrane integrity and become more permeable, leading to leakage of

481 periplasmic and cytoplasmic proteins (Fig. 7). Although Sec and Tat pathways are
482 mechanistically distinct, a few proteins can be targeted by either pathway, showing the
483 flexibility of their target signal peptides[6]. Crosstalk is evident in quality control and regulatory
484 processes, where overproduction or dysfunction in any part of the pathway can affect
485 others[16]. This interplay ensures bacteria balance the secretion systems for various proteins
486 crucial for virulence, adaptation, and cellular physiology.

487 ## Materials and Methods

488 ### Bacterial strains and plasmids used for the study

489 *Mtb H37Rv* (*Rv*), a pathogenic laboratory strain sensitive to all antibiotics, was used in
490 this study. Conditional knockdown strains *Rv-secA1*$_{dc}$, *Rv-tatA*$_{dc}$, and complementation strains
491 were generated by electroporating relevant constructs into *Rv*. The pTetIntdCas9 plasmid
492 used in this study has dCas9 under tetracycline (ATc) inducible promoter, L5 integrative site,
493 which was described previously[44]. Two guide RNAs each were designed to achieve sufficient
494 depletion upon the addition of ATc. *sec1144* and *sec1183* are the guide RNA sequences
495 aimed at targeting *secA1,* and *tat1142* and *tat1181* are two guide RNA sequences for *tatA*.
496 Two guide RNAs, each of 20 nucleotides complementary sequence for each target gene from
497 5'UTR and after the PAM sequence 5'NGG3' were cloned into the pTetIntdCas9 vector pTet-
498 dC-SecA1 and pTet-dC-TatA (Fig. S3a & b). The expression of dCas9 and the target sequence-
499 specific guide RNAs, both under Tet inducible promoter, halts the RNAP from proceeding
500 with transcription; hence, the target gene's knockdown occurs (Fig. S3c). For
501 complementation, the *secA1* or *tatA* (*tatA*$_{gmut}$) were mutated (Fig. S3d) such that the guide
502 RNA binding is abrogated. *secA1*$_{gmut}$ and its native promoter were amplified separately,
503 digested and cloned into pSNG-S vector containing giles attP and Integrase (unpublished) to
504 generate pSNG-secA1$_{gmut.}$ *tatA*$_{gmut}$ along with downstream *tatC* and their native promoter,
505 were amplified separately (Fig. S3d), digested and cloned into pSNG-S vector to generate
506 pSNG-tatAC$_{gmut}$.

507 ### Lysate preparation and Western blots

508 *Rv-vc*$_{dc}$, *Rv-secA1*$_{dc}$, *Rv-tatA*$_{dc}$ strains were grown until A_{600} ~0.8, and whole cell lysate
509 (WCL) was prepared by resuspending the cell pellet in lysis buffer (1x PBSG, 1x PMSF, and PIC:
510 Protease Inhibitor Cocktail). The cells were lysed using bead beating (8-10 cycles, 1 min ON
511 and 2 min OFF). The cells were centrifuged at 13000 rpm for 10 min at 4°C, and the
512 supernatant was estimated using the BCA reagent (Thermo-Fischer). 40 µg of the WCLs were
513 resolved on 10% (for SecA1) or 15% (for TatA) SDS-PAGE gels, transferred to nitrocellulose
514 membranes, and probed with α-SecA1 or α-TatA, or α-GroEL1 antibodies raised in the lab.

515

516 **RNA isolation and qRT-PCR**

517 The *Rv-vc$_{dc}$, Rv-secA1$_{dc}$, and Rv-tatA$_{dc}$* strains, with or without ATc, were grown until
518 A_{600} ~0.8, and cells equivalent to 10 O.D. were harvested after 3 days of ATc treatment. The
519 cell pellets were resuspended in 1 ml of Trizol (Invitrogen), and cells were lysed by bead
520 beating (3 rounds of 30 sec ON and 2 min OFF). The cells were centrifuged at 13000 rpm for
521 10 min at 4°C, and 300 µl of chloroform was added to the supernatants. The samples were
522 vortexed, centrifuged, and the aqueous layer containing RNA was precipitated. The pellet was
523 resuspended in RNase-free water, treated with DNase I (Invitrogen), and purified using a
524 Qiagen column. 1 µg of RNA was reverse transcribed using the iScript cDNA synthesis kit
525 (Bio-Rad). Quantitative real-time PCR was performed with iTaq Universal SYBR Green
526 Supermix (Bio-Rad) on the QuantStudio 3 system (Applied Biosystems). Data were normalized
527 to 16S rRNA expression levels. The ΔΔCt algorithm was used to evaluate the relative fold
528 change in gene expression.

529 **Bacterial survival *in vitro* and upon *ex vivo* peritoneal macrophage infection**

530 The strains were inoculated at A_{600} ~0.1 in the presence and absence of ATc. The CFUs
531 were enumerated on day 0 (data not shown) and day 4. Colonies were calculated and plotted
532 using GraphPad Prism. For the *ex vivo* infections, peritoneal macrophages were used. Briefly,
533 thioglycolate was injected into the mouse peritoneum, and macrophages were isolated 4 days
534 post-injection (Fig. 4d). 3 x 10^5 cells were seeded per well, and infection was performed at a
535 1:5 (macrophage:bacterial cells) MOI. CFUs were enumerated at 4 and 72 h post-infection
536 with and without ATc. Colonies were counted, and a graph was plotted using GraphPad Prism.

537 **Reconstruction of Secretory systems in *Mtb***

538 Inspired by the work by Feizi *et al.* on genome-scale reconstruction of protein secretion
539 system in yeast *Saccharomyces cerevisiae*, we created a manually curated reconstruction of
540 the secretion systems in *Mtb*[52]. Note that yeast is a eukaryote while *Mtb* is a bacterium. To
541 this end, a systematic manual curation of existing literature on bacterial secretion systems,
542 supported by both experimental and/or computational evidence, was performed as depicted
543 in the workflow[52,76] (Fig. 1a). Based on the compiled evidence, components of secretion
544 pathways namely, Sec dependent (SRP dependent, SecA1 dependent, and SecA2 dependent),

545 Sec independent (Tat), and T7SS were collated and annotated (Table S1 and S2). Further, the
546 protein signatures relevant for secretion and localization, such as presence or absence of
547 signal peptide sequences, lipo motif (LM), transmembrane domain (TMD), etc. were assigned
548 using the computational tools SignalP v6.0[77], Phobius v10.1 (https://phobius.sbc.su.se/),
549 DeepTMHMM v1.0 (https://services.healthtech.dtu.dk/services/DeepTMHMM-1.0/) and
550 PcnsHub[78], facilitating the identification and classification of secreted proteins (Fig. 1a).
551 Detailed mechanistic information from the existing literature was used to further organize the
552 secretion process into a series of pseudo-chemical reactions, similar to reactions formulated
553 by Feizi *et al.* for classical secretion pathway in Yeast[52]. A pictorial representation of these
554 reactions was created using Biorender (Fig. 2, Fig. S1 & S2).

555 To explore the transcriptional regulatory control of secretory components, the publicly
556 available ChIP-Seq data[40] for *Mtb* transcription factors (TFs) was used to determine the TFs
557 directly controlling the different *Mtb* secretory components (Fig. 3, Table S3). A visualization
558 of TFs controlling the *Mtb* secretory components was generated using the R package ggplot2
559 (https://ggplot2.tidyverse.org/). The gene-level expression changes of the secretory
560 components under different stress conditions were obtained from a transcriptome study
561 performed by Khan et al., 2024[42]. The differential expression was viewed using a heatmap
562 constructed using R package, pheatmap (https://cran.r-
563 project.org/web/packages/pheatmap/index.html).

564 **Culture filtrate protein preparation**

565 To isolate the culture filtrate (CF) proteins from *Mtb*, *Rv-vc*$_{dc}$, *Rv-secA1*$_{dc}$, and *Rv-tatA*$_{dc}$
566 were grown till early log-phase culture with and without ATc (500 ng/mL) in Sauton's media
567 in quadruplets[45]. Briefly, the cells were harvested and centrifuged at 4000 rpm for 10 min at
568 4˚C. The supernatants were collected into a fresh 50 mL falcon, and pellets were kept aside
569 for preparation of WCL (WCL: Whole Cell Lysate). The supernatants were centrifuged again
570 following the same condition and repeated twice. The supernatants were collected and
571 passed through a 0.2 µm syringe filter at the last centrifuge. The filtered supernatants (CF
572 proteins) were concentrated using 3 kDa Amicon centricons (~150 mL CF to 1 mL) and stored
573 at -80˚C.

574 **Secretome sample preparation for Mass spectrometry**

575 For mass spectrometry of CF proteins, 100 µg were taken into fresh low protein binding
576 MCTs (microcentrifuge tubes), and 6X volume of ice-cold acetone was added for overnight
577 precipitation at -20˚C. The samples were centrifuged at 13000 rpm for 10 min at 4˚C,
578 supernatant was discarded, and the pellets were dried in a speed vacuum. 100 µl resuspension
579 buffer containing 8M urea and 25 mM ammonium bicarbonate was added to the dry pellet,
580 and the sample was resuspended by vortexing for 30 min at RT. 10 mM of TCEP was added
581 to the tubes and incubated at RT for 30 min. 25 mM of IAA was added to the tubes and
582 incubated at RT for 30 min at dark. The proteins were then subjected to trypsin digestion
583 (Trypsin: protein - 1:20) at 37˚C overnight. The peptides were desalted using C-18, eluted in
584 a fresh MCT, and stored at -80°C.

585 **Protocol for isolation of membrane and cytosolic fractions**

586 *Rv-vc*$_{dc}$, *Rv-secA1*$_{dc}$, and *Rv-tatA*$_{dc}$ were grown in the presence and absence of ATc
587 (500 ng/mL) in 7H9+OADC media in quadruplets. On the fourth day, the cells were pelleted
588 and resuspended in lysis buffer (1x PBSG, 1x PMSF, and PIC: Protease Inhibitor Cocktail), and
589 cell lysates were prepared using bead beating for eight rounds (1 min ON and 2 min OFF
590 cycles on ice). Samples were centrifuged at 13000 rpm for 10 min at 4˚C. The supernatant was
591 collected and subjected to ultracentrifugation at 100000X g for two h at 4˚C. After the first
592 round of ultracentrifugation, the supernatant was collected and designated as the Cytosolic
593 fraction (C). The pellets were resuspended in 1x PBSG with 1X PMSF and subjected to another
594 two rounds of ultracentrifugation to collect the membrane fractions (M). After the final (third)
595 round of ultracentrifugation, the pellets (M) were resuspended in resuspension buffer (5%
596 SDS, 0.1M Tris-Cl pH-8.5) and stored at -80°C.

597 **MS Sample preparation and processing**

598 25 µg of proteins from the membrane and cytosolic fractions were reduced and
599 alkylated using 5 mM TCEP and 50 mM iodoacetamide separately. Trypsin was then added at
600 a ratio of 1:50 in µg to lysate and incubated at 37°C for 16 h. A C-18 silica cartridge was used
601 to purify the digested peptide, and a speed vacuum was used to dry it. Buffer A (2%
602 acetonitrile + 0.1% formic acid) was used to suspend the dry pellet and submitted to a mass

603 spectrometer containing an Easy-nLC-1000 system connected to an Orbitrap Exploris. The C-
604 18 column (15 cm/1.9 µm) was loaded with 1 µg peptide and was later separated as a gradient
605 using buffer B (80% acetonitrile + 0.1% formic acid) and a flow rate of 500 nL/min. The
606 duration of the LC gradients was 110 min. The eluate was injected for MS analysis. The MS1
607 spectra were obtained (Max IT = 60ms, AGQ goal = 300%; RF Lens = 70%; R=60K, mass range
608 = 375−1500; profile data). All charge states for a certain precursor were excluded for 30 sec
609 using dynamic exclusion. The top 20 peptides' MS2 spectra were gathered using the following
610 parameters: AGC target 100%, R = 15K, and Max IT = 60ms.

611 **Mass spectrometry data analysis and visualization**

612 RAW files were annotated using Proteome Discoverer 2.5 with UniProt database[79]. The
613 precursor and fragment mass limitations of 10 ppm and 0.02 Da were set for dual Sequest
614 and Amanda searches. The trypsin/P enzyme specificity of the protease was set for cleavage
615 at the C terminus of "K/R: unless followed by "P". The protein false discovery rate (FDR) and
616 peptide spectrum match (PSM) were set at 0.01. Further analysis was carried out by mapping
617 the peptide sequence obtained in culture filtrate and membrane fraction to the respective
618 UniProt ID, and LFQ values were obtained from MaxQuant[80].

619 Mycobrowser[30] database was used for creating a list of *Mtb* proteins with their
620 respective UniProt ID, Locus ID and functional classification, and was augmented with
621 information on the presence or absence of signal peptide, transmembrane helices and non-
622 classical secretion obtained by *in silico* prediction using the protein sequences from
623 Mycobrowser and computational tools SignalP v 6.0[77], DeepTMHMM v 1.0
624 (https://services.healthtech.dtu.dk/services/DeepTMHMM-1.0/), Phobius v 10.1
625 (https://phobius.sbc.su.se/) and PncsHub[78]. The UniProt IDs and the LFQ values obtained from
626 MS data were mapped with the list. The proteins having ≤2 unique peptides were removed.
627 In a similar fashion, the membrane proteome data was mapped with the created list. After
628 filtration, the proteins and LFQ values were log normalized and the differential abundance
629 was performed using limma[81] and significant proteins were considered for further analysis.

630 The differential abundance, signal peptide distribution and functional annotation were
631 visualized using pheatmap (https://cran.r-project.org/web/packages/pheatmap/index.html),

632 while volcano plots, alluvial plots and chord plots were generated using ggplot2
633 (https://ggplot2.tidyverse.org/), ggalluvial[82], and circlize[83]packages respectively in R.

634 **Scanning Electron Microscopy (SEM)**

635 For SEM, 5 mL cells at A_{600} ~0.5 of *Rv-vc*$_{dc}$, *Rv-secA1*$_{dc}$, *Rv-secA1*$_{dc}$*:: secA1, Rv-tatA*$_{dc}$,
636 and *Rv-tatA*$_{dc}$*::tatAC* were centrifuged at 4000 rpm for 10 min at RT. The supernatant was
637 discarded, and the pellets were resuspended in fixative. The cells were incubated at 37°C. The
638 cells were centrifuged for 10 min, and the pellets were washed twice with 0.1 M Na-
639 Cacodylate buffer. The cells were resuspended in 1% OsO_4 (Osmium tetroxide) and incubated
640 at RT for 90 min in a twirler. The cells were centrifuged again for 10 min at RT. The supernatant
641 was discarded, and dehydration was performed gradually with different concentrations of
642 ethanol: 25% ethanol for 5 min, 50% ethanol for 7 min, 75% ethanol for 10 min, 95% ethanol
643 for 20 min, and 100% ethanol for 30 min, three times. After each step, samples were
644 centrifuged for 10 min at RT. The pellets were resuspended in HMDS (Hexamethyldisilazane).
645 The samples were subjected to gold coating followed by SEM (S3400N, Hitachi) imaging. Cell
646 lengths were calculated using ImageJ software, and the data were plotted using GraphPad
647 Prism.

648 **Transmission Electron Microscopy (TEM)**

649 For TEM sample preparation, the SEM protocol mentioned above was followed until
650 the dehydration step. After that, the pellets were resuspended in propylene oxide and
651 incubated at 4˚C for 1-2 h on a rotator. The samples were spun down, and the supernatant
652 was discarded. A mixture of propylene oxide and resin in a 1:1 ratio was added to the samples,
653 which were then incubated at 4˚C for 2 h in a rotator. This step was repeated with 1:2 and 1:3
654 propylene oxide to resin ratios, respectively. Finally, pure resin was added to the samples and
655 incubated overnight at 4˚C on a rotator. The next day, the resin was discarded, and pure resin
656 was added to the samples, which were incubated at 60˚C for 2 h. The samples were then
657 subjected to microtome for transverse sectioning at 70 nm thickness. The sections were
658 stained with uranyl acetate, and images were taken using TEM (Talos L120c, Thermo Fischer
659 Scientific).

660 **Ethidium bromide (EtBr) uptake assay**

661 *Rv-vc$_{dc}$, Rv-secA1$_{dc}$, Rv-secA1$_{dc}$::secA1, Rv-tatA$_{dc}$,* and *Rv-tatA$_{dc}$::tatAC* strains were
662 inoculated at A_{600} ~0.1 with and without ATc. The cells were then harvested on day 2 and day
663 4 for the EtBr uptake assay. The cell pellets were washed with 1 X $PBST_{80}$. Cells at A_{600} ~0.5
664 were drawn from the cultures in an MCT, and 1 µg/ml of EtBr was added to the cultures. The
665 cultures were incubated at 37˚C for 15 min (data not shown) and 30 min in a standing
666 incubator in the dark. After incubation, the cells were washed with 1 x $PBST_{80}$ twice to remove
667 the residual EtBr. After the second wash, the pellets were resuspended in 4%
668 paraformaldehyde (PFA) for fixation. The cell suspensions were transferred into a 96-well plate
669 to take the fluorescence reading. The cell suspensions were excited at 510 nm, and the
670 emission spectra were collected at 595 nm. Without EtBr, added cells were taken as a control
671 to normalize and get the absolute unit (A.U.) value using GraphPad Prism software.

672 **Propidium Iodide (PI) uptake assay**

673 *Rv-vc$_{dc}$, Rv-secA1$_{dc}$, Rv-secA1$_{dc}$::secA1, Rv-tatA$_{dc}$, and Rv-tatA$_{dc}$::tatAC* strains were
674 grown in the presence and absence of ATc. On Day 2 and Day 4, the cells were processed for
675 a PI uptake assay. The cells were washed with 1 X $PBST_{80}$. A volume of 5 µg/ml of PI was added
676 to cells at A_{600} ~0.5 and incubated at 37˚C for 5 min in a standing incubator in the dark. After
677 incubation, the cells were washed twice with 1X $PBST_{80}$ to remove any residual PI. The cells
678 were then resuspended in 4% paraformaldehyde (PFA). The cell suspension was used for flow
679 cytometry analysis. The fluorescence of the PI-containing cells was plotted using GraphPad
680 Prism.

681 **Resource Availability**

682 **Lead contact**

683 Reagent inquiries will be directed to, and fulfilled by, the lead contact, Dr. Vinay Kumar
684 Nandicoori (vinaykn.ccmb@csir.res.in).

685 **Materials availability**

686 The materials generated in this study are available from the lead contact with a completed
687 materials transfer agreement.

688 **Data and code availability**

The mass spectrometry data generated in this study have been deposited to PRIDE: PXD066777.

Any additional information required to reanalyse the data reported in this paper is available from the lead contact upon request.

Acknowledgement

Research in this publication was supported by JC Bose Award (JCB/2019/000015), Govt. of India to VKN. VKN and JU acknowledges the support from Department of Biotechnology (DBT) (Grant No. BT/PR50983/MED/29/1650/2023). VKN, PS and YB acknowledge the support from National Institute of Health (NIH) (Grant No. 7R01A|142672-05). AS acknowledges funding from the Department of Atomic Energy (DAE), Government of India, via Apex project to The Institute of Mathematical Sciences (IMSc), Chennai. PS is INSPIRE Fellow from Department of Science & Technology (DST), Government of India (DST/INSPIRE Fellowship/2018/F180904). We are grateful to A. Harikrishna, CSIR-Centre for Cellular and Molecular Biology (CCMB) for his assistance in microtome and TEM image acquisition. We thank CCMB central research facilities: DNA Sequencing, BSL-3, Tissue Culture, Animal House (IAEC-25/2023) and Electron Microscopy, for providing access. Portions of the abstract and cover letter were refined for style and grammar with the assistance of ChatGPT (OpenAI; August 2025). The authors reviewed and edited all text and accept full responsibility for the content. No AI tools were used to generate or alter data, analyses, results, or figures/images.

Declaration of Interest

The authors declare no competing interests.

711 **References**

712 1. Muniz, M., Morsomme, P., and Riezman, H. (2001). Protein sorting upon exit from the
713 endoplasmic reticulum. Cell *104*, 313-320. 10.1016/s0092-8674(01)00215-x.
714 2. Wickner, W., Driessen, A.J., and Hartl, F.U. (1991). The enzymology of protein
715 translocation across the Escherichia coli plasma membrane. Annu Rev Biochem *60*,
716 101-124. 10.1146/annurev.bi.60.070191.000533.
717 3. Driessen, A.J., Manting, E.H., and van der Does, C. (2001). The structural basis of protein
718 targeting and translocation in bacteria. Nat Struct Biol *8*, 492-498. 10.1038/88549.
719 4. Berks, B.C., Palmer, T., and Sargent, F. (2005). Protein targeting by the bacterial twin-
720 arginine translocation (Tat) pathway. Curr Opin Microbiol *8*, 174-181.
721 10.1016/j.mib.2005.02.010.
722 5. Fan, E., Jakob, M., and Klosgen, R.B. (2010). One signal is enough: Stepwise transport
723 of two distinct passenger proteins by the Tat pathway across the thylakoid membrane.
724 Biochem Biophys Res Commun *398*, 438-443. 10.1016/j.bbrc.2010.06.095.
725 6. Natale, P., Bruser, T., and Driessen, A.J. (2008). Sec- and Tat-mediated protein secretion
726 across the bacterial cytoplasmic membrane--distinct translocases and mechanisms.
727 Biochim Biophys Acta *1778*, 1735-1756. 10.1016/j.bbamem.2007.07.015.
728 7. Feltcher, M.E., Sullivan, J.T., and Braunstein, M. (2010). Protein export systems of
729 Mycobacterium tuberculosis: novel targets for drug development? Future Microbiol *5*,
730 1581-1597. 10.2217/fmb.10.112.
731 8. Chatzi, K.E., Sardis, M.F., Tsirigotaki, A., Koukaki, M., Sostaric, N., Konijnenberg, A.,
732 Sobott, F., Kalodimos, C.G., Karamanou, S., and Economou, A. (2017). Preprotein mature
733 domains contain translocase targeting signals that are essential for secretion. J Cell
734 Biol *216*, 1357-1369. 10.1083/jcb.201609022.
735 9. Miller, B.K., Zulauf, K.E., and Braunstein, M. (2017). The Sec Pathways and Exportomes
736 of Mycobacterium tuberculosis. Microbiol Spectr *5*. 10.1128/microbiolspec.TBTB2-
737 0013-2016.
738 10. Champion, P.A., and Cox, J.S. (2007). Protein secretion systems in Mycobacteria. Cell
739 Microbiol *9*, 1376-1384. 10.1111/j.1462-5822.2007.00943.x.
740 11. Ligon, L.S., Rigel, N.W., Romanchuk, A., Jones, C.D., and Braunstein, M. (2013).
741 Suppressor analysis reveals a role for SecY in the SecA2-dependent protein export
742 pathway of Mycobacteria. J Bacteriol *195*, 4456-4465. 10.1128/JB.00630-13.
743 12. Thakur, P., Gantasala, N.P., Choudhary, E., Singh, N., Abdin, M.Z., and Agarwal, N. (2016).
744 The preprotein translocase YidC controls respiratory metabolism in Mycobacterium
745 tuberculosis. Sci Rep *6*, 24998. 10.1038/srep24998.
746 13. Hou, J.M., D'Lima, N.G., Rigel, N.W., Gibbons, H.S., McCann, J.R., Braunstein, M., and
747 Teschke, C.M. (2008). ATPase activity of Mycobacterium tuberculosis SecA1 and SecA2
748 proteins and its importance for SecA2 function in macrophages. J Bacteriol *190*, 4880-
749 4887. 10.1128/JB.00412-08.
750 14. Ollinger, J., O'Malley, T., Ahn, J., Odingo, J., and Parish, T. (2012). Inhibition of the sole
751 type I signal peptidase of Mycobacterium tuberculosis is bactericidal under replicating
752 and nonreplicating conditions. J Bacteriol *194*, 2614-2619. 10.1128/JB.00224-12.

753 15. Frobel, J., Rose, P., and Muller, M. (2012). Twin-arginine-dependent translocation of
754 folded proteins. Philos Trans R Soc Lond B Biol Sci *367*, 1029-1046.
755 10.1098/rstb.2011.0202.
756 16. Frain, K.M., Robinson, C., and van Dijl, J.M. (2019). Transport of Folded Proteins by the
757 Tat System. Protein J *38*, 377-388. 10.1007/s10930-019-09859-y.
758 17. McDonough, J.A., McCann, J.R., Tekippe, E.M., Silverman, J.S., Rigel, N.W., and
759 Braunstein, M. (2008). Identification of functional Tat signal sequences in
760 Mycobacterium tuberculosis proteins. J Bacteriol *190*, 6428-6438. 10.1128/JB.00749-
761 08.
762 18. Ize, B., Stanley, N.R., Buchanan, G., and Palmer, T. (2003). Role of the Escherichia coli
763 Tat pathway in outer membrane integrity. Mol Microbiol *48*, 1183-1193.
764 10.1046/j.1365-2958.2003.03504.x.
765 19. Braunstein, M., Brown, A.M., Kurtz, S., and Jacobs, W.R., Jr. (2001). Two nonredundant
766 SecA homologues function in mycobacteria. J Bacteriol *183*, 6979-6990.
767 10.1128/JB.183.24.6979-6990.2001.
768 20. Swanson, S., Ioerger, T.R., Rigel, N.W., Miller, B.K., Braunstein, M., and Sacchettini, J.C.
769 (2015). Structural Similarities and Differences between Two Functionally Distinct SecA
770 Proteins, Mycobacterium tuberculosis SecA1 and SecA2. J Bacteriol *198*, 720-730.
771 10.1128/JB.00696-15.
772 21. Braunstein, M., Espinosa, B.J., Chan, J., Belisle, J.T., and Jacobs, W.R., Jr. (2003). SecA2
773 functions in the secretion of superoxide dismutase A and in the virulence of
774 Mycobacterium tuberculosis. Mol Microbiol *48*, 453-464. 10.1046/j.1365-
775 2958.2003.03438.x.
776 22. Feltcher, M.E., Gunawardena, H.P., Zulauf, K.E., Malik, S., Griffin, J.E., Sassetti, C.M., Chen,
777 X., and Braunstein, M. (2015). Label-free Quantitative Proteomics Reveals a Role for the
778 Mycobacterium tuberculosis SecA2 Pathway in Exporting Solute Binding Proteins and
779 Mce Transporters to the Cell Wall. Mol Cell Proteomics *14*, 1501-1516.
780 10.1074/mcp.M114.044685.
781 23. Lochab, S., Singh, Y., Sengupta, S., and Nandicoori, V.K. (2020). Mycobacterium
782 tuberculosis exploits host ATM kinase for survival advantage through SecA2
783 secretome. Elife *9*. 10.7554/eLife.51466.
784 24. Zulauf, K.E., Sullivan, J.T., and Braunstein, M. (2018). The SecA2 pathway of
785 Mycobacterium tuberculosis exports effectors that work in concert to arrest
786 phagosome and autophagosome maturation. PLoS Pathog *14*, e1007011.
787 10.1371/journal.ppat.1007011.
788 25. Zhou, W., Hao, B., Bricker, T.M., and Theg, S.M. (2023). A real-time analysis of protein
789 transport via the twin arginine translocation pathway in response to different
790 components of the protonmotive force. J Biol Chem *299*, 105286.
791 10.1016/j.jbc.2023.105286.
792 26. Rivera-Calzada, A., Famelis, N., Llorca, O., and Geibel, S. (2021). Type VII secretion
793 systems: structure, functions and transport models. Nat Rev Microbiol *19*, 567-584.
794 10.1038/s41579-021-00560-5.

795 27. Unnikrishnan, M., Constantinidou, C., Palmer, T., and Pallen, M.J. (2017). The Enigmatic
796 Esx Proteins: Looking Beyond Mycobacteria. Trends Microbiol *25*, 192-204.
797 10.1016/j.tim.2016.11.004.
798 28. Roy, S., Ghatak, D., Das, P., and BoseDasgupta, S. (2020). ESX secretion system: The
799 gatekeepers of mycobacterial survivability and pathogenesis. Eur J Microbiol Immunol
800 (Bp) *10*, 202-209. 10.1556/1886.2020.00028.
801 29. Sankey, N., Merrick, H., Singh, P., Rogers, J., Reddi, A., Hartson, S.D., and Mitra, A. (2023).
802 Role of the Mycobacterium tuberculosis ESX-4 Secretion System in Heme Iron
803 Utilization and Pore Formation by PPE Proteins. mSphere *8*, e0057322.
804 10.1128/msphere.00573-22.
805 30. Kapopoulou, A., Lew, J.M., and Cole, S.T. (2011). The MycoBrowser portal: a
806 comprehensive and manually annotated resource for mycobacterial genomes.
807 Tuberculosis (Edinb) *91*, 8-13. 10.1016/j.tube.2010.09.006.
808 31. van der Woude, A.D., Stoop, E.J., Stiess, M., Wang, S., Ummels, R., van Stempvoort, G.,
809 Piersma, S.R., Cascioferro, A., Jimenez, C.R., Houben, E.N., et al. (2014). Analysis of
810 SecA2-dependent substrates in Mycobacterium marinum identifies protein kinase G
811 (PknG) as a virulence effector. Cell Microbiol *16*, 280-295. 10.1111/cmi.12221.
812 32. Miller, B.K., Hughes, R., Ligon, L.S., Rigel, N.W., Malik, S., Anjuwon-Foster, B.R.,
813 Sacchettini, J.C., and Braunstein, M. (2019). Mycobacterium tuberculosis SatS is a
814 chaperone for the SecA2 protein export pathway. Elife *8*. 10.7554/eLife.40063.
815 33. Braunstein, M., Bensing, B.A., and Sullam, P.M. (2019). The Two Distinct Types of SecA2-
816 Dependent Export Systems. Microbiol Spectr *7*. 10.1128/microbiolspec.PSIB-0025-
817 2018.
818 34. Prabudiansyah, I., Kusters, I., and Driessen, A.J. (2015). In Vitro Interaction of the
819 Housekeeping SecA1 with the Accessory SecA2 Protein of Mycobacterium
820 tuberculosis. PLoS One *10*, e0128788. 10.1371/journal.pone.0128788.
821 35. Pal, R., Bisht, M.K., and Mukhopadhyay, S. (2022). Secretory proteins of Mycobacterium
822 tuberculosis and their roles in modulation of host immune responses: focus on
823 therapeutic targets. FEBS J *289*, 4146-4171. 10.1111/febs.16369.
824 36. Abdallah, A.M., Bestebroer, J., Savage, N.D., de Punder, K., van Zon, M., Wilson, L.,
825 Korbee, C.J., van der Sar, A.M., Ottenhoff, T.H., van der Wel, N.N., et al. (2011).
826 Mycobacterial secretion systems ESX-1 and ESX-5 play distinct roles in host cell death
827 and inflammasome activation. J Immunol *187*, 4744-4753. 10.4049/jimmunol.1101457.
828 37. Tran, H.R., Grebenc, D.W., Klein, T.A., and Whitney, J.C. (2021). Bacterial type VII
829 secretion: An important player in host-microbe and microbe-microbe interactions. Mol
830 Microbiol *115*, 478-489. 10.1111/mmi.14680.
831 38. Groschel, M.I., Sayes, F., Simeone, R., Majlessi, L., and Brosch, R. (2016). ESX secretion
832 systems: mycobacterial evolution to counter host immunity. Nat Rev Microbiol *14*, 677-
833 691. 10.1038/nrmicro.2016.131.
834 39. Cronin, R.M., Ferrell, M.J., Cahir, C.W., Champion, M.M., and Champion, P.A. (2022).
835 Proteo-genetic analysis reveals clear hierarchy of ESX-1 secretion in Mycobacterium
836 marinum. Proc Natl Acad Sci U S A *119*, e2123100119. 10.1073/pnas.2123100119.

837 40. Minch, K.J., Rustad, T.R., Peterson, E.J., Winkler, J., Reiss, D.J., Ma, S., Hickey, M., Brabant,
838 W., Morrison, B., Turkarslan, S., et al. (2015). The DNA-binding network of
839 Mycobacterium tuberculosis. Nat Commun *6*, 5829. 10.1038/ncomms6829.
840 41. Turkarslan, S., Peterson, E.J., Rustad, T.R., Minch, K.J., Reiss, D.J., Morrison, R., Ma, S.,
841 Price, N.D., Sherman, D.R., and Baliga, N.S. (2015). A comprehensive map of genome-
842 wide gene regulation in Mycobacterium tuberculosis. Sci Data *2*, 150010.
843 10.1038/sdata.2015.10.
844 42. Khan, M.Z., Hunt, D.M., Singha, B., Kapoor, Y., Singh, N.K., Prasad, D.V.S., Dharmarajan,
845 S., Sowpati, D.T., de Carvalho, L.P.S., and Nandicoori, V.K. (2024). Divergent downstream
846 biosynthetic pathways are supported by <sc>L</sc>-cysteine synthases of
847 Mycobacterium tuberculosis. Elife *12*. 10.7554/eLife.91970.
848 43. Kaur, P., Rausch, M., Malakar, B., Watson, U., Damle, N.P., Chawla, Y., Srinivasan, S.,
849 Sharma, K., Schneider, T., Jhingan, G.D., et al. (2019). LipidII interaction with specific
850 residues of Mycobacterium tuberculosis PknB extracytoplasmic domain governs its
851 optimal activation. Nat Commun *10*, 1231. 10.1038/s41467-019-09223-9.
852 44. Choudhary, E., Thakur, P., Pareek, M., and Agarwal, N. (2015). Gene silencing by CRISPR
853 interference in mycobacteria. Nat Commun *6*, 6267. 10.1038/ncomms7267.
854 45. Sanyal, P., and Nandicoori, V.K. (2025). Preparation of Mycobacterium tuberculosis
855 Culture Filtrate to Understand TB Pathogenesis. J Vis Exp. 10.3791/67540.
856 46. Nisa, A., Counoupas, C., Pinto, R., Britton, W.J., and Triccas, J.A. (2022). Characterization
857 of the Protective Immune Responses Conferred by Recombinant BCG Overexpressing
858 Components of Mycobacterium tuberculosis Sec Protein Export System. Vaccines
859 (Basel) *10*. 10.3390/vaccines10060945.
860 47. Malen, H., Berven, F.S., Fladmark, K.E., and Wiker, H.G. (2007). Comprehensive analysis
861 of exported proteins from Mycobacterium tuberculosis H37Rv. Proteomics *7*, 1702-
862 1718. 10.1002/pmic.200600853.
863 48. de Souza, G.A., Leversen, N.A., Malen, H., and Wiker, H.G. (2011). Bacterial proteins with
864 cleaved or uncleaved signal peptides of the general secretory pathway. J Proteomics
865 *75*, 502-510. 10.1016/j.jprot.2011.08.016.
866 49. Mehra, A., Zahra, A., Thompson, V., Sirisaengtaksin, N., Wells, A., Porto, M., Koster, S.,
867 Penberthy, K., Kubota, Y., Dricot, A., et al. (2013). Mycobacterium tuberculosis type VII
868 secreted effector EsxH targets host ESCRT to impair trafficking. PLoS Pathog *9*,
869 e1003734. 10.1371/journal.ppat.1003734.
870 50. Malakar, B., Chauhan, K., Sanyal, P., Naz, S., Kalam, H., Vivek-Ananth, R.P., Singh, L.V.,
871 Samal, A., Kumar, D., and Nandicoori, V.K. (2023). Phosphorylation of CFP10 modulates
872 Mycobacterium tuberculosis virulence. mBio *14*, e0123223. 10.1128/mbio.01232-23.
873 51. Palande, A., Patil, S., Veeram, A., Sahoo, S.S., Lodhiya, T., Maurya, P., Muralikrishnan, B.,
874 Chugh, J., and Mukherjee, R. (2024). Proteomic Analysis of the Mycobacterium
875 tuberculosis Outer Membrane for Potential Implications in Uptake of Small Molecules.
876 ACS Infect Dis *10*, 890-906. 10.1021/acsinfecdis.3c00517.
877 52. Feizi, A., Osterlund, T., Petranovic, D., Bordel, S., and Nielsen, J. (2013). Genome-scale
878 modeling of the protein secretory machinery in yeast. PLoS One *8*, e63284.
879 10.1371/journal.pone.0063284.

880 53. Celinska, E., and Nicaud, J.M. (2019). Filamentous fungi-like secretory pathway strayed
881 in a yeast system: peculiarities of Yarrowia lipolytica secretory pathway underlying its
882 extraordinary performance. Appl Microbiol Biotechnol *103*, 39-52. 10.1007/s00253-
883 018-9450-2.
884 54. Feizi, A., Gatto, F., Uhlen, M., and Nielsen, J. (2017). Human protein secretory pathway
885 genes are expressed in a tissue-specific pattern to match processing demands of the
886 secretome. NPJ Syst Biol Appl *3*, 22. 10.1038/s41540-017-0021-4.
887 55. Gutierrez, J.M., Feizi, A., Li, S., Kallehauge, T.B., Hefzi, H., Grav, L.M., Ley, D., Baycin Hizal,
888 D., Betenbaugh, M.J., Voldborg, B., et al. (2020). Genome-scale reconstructions of the
889 mammalian secretory pathway predict metabolic costs and limitations of protein
890 secretion. Nat Commun *11*, 68. 10.1038/s41467-019-13867-y.
891 56. Sertbas, M., and Ulgen, K.O. (2020). Genome-Scale Metabolic Modeling for Unraveling
892 Molecular Mechanisms of High Threat Pathogens. Front Cell Dev Biol *8*, 566702.
893 10.3389/fcell.2020.566702.
894 57. Durot, M., Bourguignon, P.Y., and Schachter, V. (2009). Genome-scale models of
895 bacterial metabolism: reconstruction and applications. FEMS Microbiol Rev *33*, 164-
896 190. 10.1111/j.1574-6976.2008.00146.x.
897 58. Passi, A., Tibocha-Bonilla, J.D., Kumar, M., Tec-Campos, D., Zengler, K., and Zuniga, C.
898 (2021). Genome-Scale Metabolic Modeling Enables In-Depth Understanding of Big
899 Data. Metabolites *12*. 10.3390/metabo12010014.
900 59. Bordbar, A., Lewis, N.E., Schellenberger, J., Palsson, B.O., and Jamshidi, N. (2010). Insight
901 into human alveolar macrophage and M. tuberculosis interactions via metabolic
902 reconstructions. Mol Syst Biol *6*, 422. 10.1038/msb.2010.68.
903 60. Beste, D.J., Hooper, T., Stewart, G., Bonde, B., Avignone-Rossa, C., Bushell, M.E.,
904 Wheeler, P., Klamt, S., Kierzek, A.M., and McFadden, J. (2007). GSMN-TB: a web-based
905 genome-scale network model of Mycobacterium tuberculosis metabolism. Genome
906 Biol *8*, R89. 10.1186/gb-2007-8-5-r89.
907 61. Kavvas, E.S., Seif, Y., Yurkovich, J.T., Norsigian, C., Poudel, S., Greenwald, W.W., Ghatak,
908 S., Palsson, B.O., and Monk, J.M. (2018). Updated and standardized genome-scale
909 reconstruction of Mycobacterium tuberculosis H37Rv, iEK1011, simulates flux states
910 indicative of physiological conditions. BMC Syst Biol *12*, 25. 10.1186/s12918-018-0557-
911 y.
912 62. Lopez-Agudelo, V.A., Mendum, T.A., Laing, E., Wu, H., Baena, A., Barrera, L.F., Beste,
913 D.J.V., and Rios-Estepa, R. (2020). A systematic evaluation of Mycobacterium
914 tuberculosis Genome-Scale Metabolic Networks. PLoS Comput Biol *16*, e1007533.
915 10.1371/journal.pcbi.1007533.
916 63. Orth, J.D., Conrad, T.M., Na, J., Lerman, J.A., Nam, H., Feist, A.M., and Palsson, B.O.
917 (2011). A comprehensive genome-scale reconstruction of Escherichia coli metabolism-
918 -2011. Mol Syst Biol *7*, 535. 10.1038/msb.2011.65.
919 64. Shah, S., and Briken, V. (2016). Modular Organization of the ESX-5 Secretion System in
920 Mycobacterium tuberculosis. Front Cell Infect Microbiol *6*, 49.
921 10.3389/fcimb.2016.00049.

922 65. Tsirigotaki, A., De Geyter, J., Sostaric, N., Economou, A., and Karamanou, S. (2017).
923 Protein export through the bacterial Sec pathway. Nat Rev Microbiol *15*, 21-36.
924 10.1038/nrmicro.2016.161.
925 66. Li, F., Chen, Y., Qi, Q., Wang, Y., Yuan, L., Huang, M., Elsemman, I.E., Feizi, A., Kerkhoven,
926 E.J., and Nielsen, J. (2022). Improving recombinant protein production by yeast through
927 genome-scale modeling using proteome constraints. Nat Commun *13*, 2969.
928 10.1038/s41467-022-30689-7.
929 67. Ates, L.S., Ummels, R., Commandeur, S., van de Weerd, R., Sparrius, M., Weerdenburg,
930 E., Alber, M., Kalscheuer, R., Piersma, S.R., Abdallah, A.M., et al. (2015). Essential Role of
931 the ESX-5 Secretion System in Outer Membrane Permeability of Pathogenic
932 Mycobacteria. PLoS Genet *11*, e1005190. 10.1371/journal.pgen.1005190.
933 68. Kwon, K.W., Choi, H.G., Choi, H.H., Choi, E., Kim, H., Kim, H.J., and Shin, S.J. (2024).
934 Immunogenicity and protective efficacy of RipA, a peptidoglycan hydrolase, against
935 Mycobacterium tuberculosis Beijing outbreak strains. Vaccine *42*, 1941-1952.
936 10.1016/j.vaccine.2024.02.039.
937 69. Healy, C., Gouzy, A., and Ehrt, S. (2020). Peptidoglycan Hydrolases RipA and Ami1 Are
938 Critical for Replication and Persistence of Mycobacterium tuberculosis in the Host.
939 mBio *11*. 10.1128/mBio.03315-19.
940 70. Widdick, D.A., Dilks, K., Chandra, G., Bottrill, A., Naldrett, M., Pohlschroder, M., and
941 Palmer, T. (2006). The twin-arginine translocation pathway is a major route of protein
942 export in Streptomyces coelicolor. Proc Natl Acad Sci U S A *103*, 17927-17932.
943 10.1073/pnas.0607025103.
944 71. McDonough, J.A., Hacker, K.E., Flores, A.R., Pavelka, M.S., Jr., and Braunstein, M. (2005).
945 The twin-arginine translocation pathway of Mycobacterium smegmatis is functional
946 and required for the export of mycobacterial beta-lactamases. J Bacteriol *187*, 7667-
947 7679. 10.1128/JB.187.22.7667-7679.2005.
948 72. Bellinzoni, M., Haouz, A., Miras, I., Magnet, S., Andre-Leroux, G., Mukherjee, R., Shepard,
949 W., Cole, S.T., and Alzari, P.M. (2014). Structural studies suggest a peptidoglycan
950 hydrolase function for the Mycobacterium tuberculosis Tat-secreted protein Rv2525c.
951 J Struct Biol *188*, 156-164. 10.1016/j.jsb.2014.09.003.
952 73. Wolfe, L.M., Mahaffey, S.B., Kruh, N.A., and Dobos, K.M. (2010). Proteomic definition of
953 the cell wall of Mycobacterium tuberculosis. J Proteome Res *9*, 5816-5826.
954 10.1021/pr1005873.
955 74. Malen, H., Pathak, S., Softeland, T., de Souza, G.A., and Wiker, H.G. (2010). Definition of
956 novel cell envelope associated proteins in Triton X-114 extracts of Mycobacterium
957 tuberculosis H37Rv. BMC Microbiol *10*, 132. 10.1186/1471-2180-10-132.
958 75. Gunawardena, H.P., Feltcher, M.E., Wrobel, J.A., Gu, S., Braunstein, M., and Chen, X.
959 (2013). Comparison of the membrane proteome of virulent Mycobacterium
960 tuberculosis and the attenuated Mycobacterium bovis BCG vaccine strain by label-free
961 quantitative proteomics. J Proteome Res *12*, 5463-5474. 10.1021/pr400334k.
962 76. Samal, A., Craig, J.P., Coradetti, S.T., Benz, J.P., Eddy, J.A., Price, N.D., and Glass, N.L.
963 (2017). Network reconstruction and systems analysis of plant cell wall deconstruction
964 by Neurospora crassa. Biotechnol Biofuels *10*, 225. 10.1186/s13068-017-0901-2.

965 77. Teufel, F., Almagro Armenteros, J.J., Johansen, A.R., Gislason, M.H., Pihl, S.I., Tsirigos,
966 K.D., Winther, O., Brunak, S., von Heijne, G., and Nielsen, H. (2022). SignalP 6.0 predicts
967 all five types of signal peptides using protein language models. Nat Biotechnol *40*,
968 1023-1025. 10.1038/s41587-021-01156-3.
969 78. Dai, W., Li, J., Li, Q., Cai, J., Su, J., Stubenrauch, C., and Wang, J. (2022). PncsHub: a
970 platform for annotating and analyzing non-classically secreted proteins in Gram-
971 positive bacteria. Nucleic Acids Res *50*, D848-D857. 10.1093/nar/gkab814.
972 79. UniProt, C. (2023). UniProt: the Universal Protein Knowledgebase in 2023. Nucleic Acids
973 Res *51*, D523-D531. 10.1093/nar/gkac1052.
974 80. Cox, J., and Mann, M. (2008). MaxQuant enables high peptide identification rates,
975 individualized p.p.b.-range mass accuracies and proteome-wide protein quantification.
976 Nat Biotechnol *26*, 1367-1372. 10.1038/nbt.1511.
977 81. Ritchie, M.E., Phipson, B., Wu, D., Hu, Y., Law, C.W., Shi, W., and Smyth, G.K. (2015).
978 limma powers differential expression analyses for RNA-sequencing and microarray
979 studies. Nucleic Acids Res *43*, e47. 10.1093/nar/gkv007.
980 82. Brunson, J.C. (2020). ggalluvial: Layered Grammar for Alluvial Plots. J Open Source
981 Softw *5*. 10.21105/joss.02017.
982 83. Gu, Z., Gu, L., Eils, R., Schlesner, M., and Brors, B. (2014). circlize Implements and
983 enhances circular visualization in R. Bioinformatics *30*, 2811-2812.
984 10.1093/bioinformatics/btu393.
985
986
987

988 **Figure 1: Reconstruction of Secretion pathways in *Mtb*.**

989 a) Workflow showing the steps involved in identification and annotation of components
990 associated with secretion systems in *Mtb.* The secretory components were curated manually
991 based on the experimental evidence and literature obtained from public sources. The
992 integration of publicly available ChIP-Seq and RNA-Seq data with the curated list of
993 components led to insights on regulation of secretion systems. b) Venn diagram depicting
994 the distribution of the annotated components among the generalized secretion systems (Sec
995 and Tat) and specialized (ESX1-5) secretion systems. c) *In silico* identification and
996 characterization of *Mtb* proteins based on presence or absence of N-terminal signal sequence
997 specific to secretory system, transmembrane domain (TMD) and Lipo motif (LM). The signal
998 peptides and Lipo motifs specific to Sec and Tat were predicted by using SignalP v6, motifs
999 specific to ESX system using SecretoMyc database, and transmembrane domains using
1000 DeepTMHMM 1.0 and Phobius. After prediction of signatures, the proteins were divided into
1001 the categories depicted in the flowchart. Created in BioRender. Nandicoori, V. (2025)
1002 https://BioRender.com/n39ydxs.

1003 **Figure 2: Schematic representation of secretion systems in *Mtb*.**

1004 (a) Pictorial model depicting the steps involved in secretion of a protein containing N-terminal
1005 Sec specific signal peptide using SecA1 dependent Sec pathway. (b) Steps involved in
1006 secretion of a protein containing Tat signal peptide (twin arginine -RR- motifs) using Tat
1007 pathway. (c) Overview of protein secretion using specialized secretion systems (ESX1- ESX5)
1008 in *Mtb*. The steps shown were based on the mechanistic reactions framed using the
1009 experimental evidence provided in Table S2. Created in BioRender. Nandicoori, V. (2025)
1010 https://BioRender.com/oa5201s.

1011 **Figure 3: Transcriptional regulation of components of secretion systems and differential**
1012 **expression of secretory components under different stress conditions.**

1013 (a) Radial pie chart grouping the transcription factors (TFs) based on the number of the
1014 secretory components they directly regulate. Checkerboard plots illustrating the regulation
1015 of secretory components by transcription factors. (b) TFs controlling > 4 components and (c)
1016 TFs controlling 2-4 components. Each row represents a Transcription Factor (x-axis) and each

1017 column a regulated secretory component (y-axis). The secretory components were grouped
1018 based on the three secretion systems. Common secretory components shared by the
1019 secretion systems were also shown. Presence of a filled square indicates a detected direct
1020 regulatory interaction. The ChIP-Seq data for TFs was obtained from MTB Network portal. (d)
1021 Heatmap depicting the differential expression (Log2FC) of the secretory components under
1022 different stress conditions. The differential expression values were obtained from RNA Seq
1023 data published by Khan et al., 2024.

1024 **Figure 4: Impact of bacterial survival upon *secA1* and *tatA* depletion.**

1025 a) *Rv-vc$_{dc}$*, *Rv-secA1$_{dc}$* and *Rv-tatA$_{dc}$* were inoculated at A_{600} ~0.1 and grown for 4 days in the
1026 presence and absence of ATc. The tubes represent the depletion of *Rv-secA1$_{dc}$* and *Rv-tatA$_{dc}$*
1027 as compared to *Rv-vc$_{dc}$*. b) Whole cell lysates (WCLs) were prepared from *Rv-vc$_{dc}$*+ATc, *Rv-*
1028 *secA1$_{dc}$*-/+ATc and *Rv-tatA$_{dc}$*-/+ATc from grown 4th day culture. 50 µg of each protein lysates
1029 were resolved on 10% (SecA1) 15% (TatA) SDS-PAGE, transferred on Nitrocellulose membrane
1030 and probed with α-SecA1 (for SecA1 depletion), and α-TatA (for TatA depletion) antibodies
1031 generated in the lab. α-GroEL1 antibody was used as loading control. c) Total RNA was
1032 isolated from *Rv-vc$_{dc}$* -/+ATc, *Rv-secA1$_{dc}$* -/+ATc and *Rv-tatA$_{dc}$* -/+ATc from 3rd day grown
1033 cultures for qRT-PCR. The expression of *secA1, tatA* and *tatC* were normalized with respect to
1034 16S rRNA and the Fold Change ($2^{-\Delta\Delta Ct}$) value (mean ± SD (n = 4)) was plotted using GraphPad
1035 Prism. The Statistical significant was analysed using One-way ANOVA, ***, $p < 0.0001$. d) The
1036 graph depicts the CFU of the *in vitro* survival of bacteria of *Rv-vc$_{dc}$* -/+ATc, *Rv-secA1$_{dc}$*-/+ATc,
1037 *Rv-secA1$_{dc}$::secA1* -/+ATc, *Rv-tatA$_{dc}$*-/+ATc and *Rv-tatA$_{dc}$::tatAC* -/+ATc on 4th day post
1038 depletion. GraphPad Prism software was used to plot CFUs and performed statistical analysis
1039 using One way ANOVA. Three independent experiments were performed as biological
1040 replicates and each experiment was conducted in triplicates. Data represents mean and ± SD,
1041 **** $p<0.0001$. e) Schematic representation of peritoneal macrophages isolation from mice
1042 peritoneum. 4 days post thioglycolate injection at the mice peritoneum, the macrophages
1043 were collected, seeded for 16h and infected with the *Rv-vc$_{dc}$*, *Rv-secA1$_{dc}$*, *Rv-secA1$_{dc}$::secA1,*
1044 *Rv-tatA$_{dc}$,* and *Rv-tatA$_{dc}$::tatAC* at 1:5 MOI. 4 h post infection, CFUs were enumerated at 0h
1045 and 96h. Created in BioRender. Nandicoori, V. (2025) https://BioRender.com/xwcvl0i. f)

1046 Survival of the *Rv-vc*$_{dc}$, *Rv-secA1*$_{dc}$, *Rv-secA1*$_{dc}$*::secA1, Rv-tatA*$_{dc}$, and *Rv-tatA*$_{dc}$*::tatAC* in the
1047 present and absence of ATc. GraphPad Prism software was used to plot CFUs and performed
1048 statistical analysis using One way ANOVA. Three independent experiments were performed
1049 as biological replicates and each experiment was conducted in triplicates. Data represents
1050 mean and ± SD, **** $p<0.0001$.

1051 **Figure 5: Secretome of SecA1 and TatAC.**

1052 a) Schematic representation of Secretome data analysis of SecA1 and TatAC. Raw data was
1053 analysed using Uniprot database. The data was screened for spectral annotation. The proteins
1054 were predicted for signal peptides for Sec, Tat and T7SS using SignalP v6, PRED-TAT and
1055 PncsHub respectively, followed by removal of transmembrane helices using DeepTMHMM
1056 1.0 and Phobius. Localization of the proteins were also checked using psortb v3.0.3. The
1057 filtered proteins were normalised and differential protein abundances were plotted. Created
1058 in BioRender. Nandicoori, V. (2025) https://BioRender.com/v0npynh. b-c) The volcano plots
1059 of SecA1 (b) and TatAC (c) depletion using $1 \geq \log_2$Fold Change≤ -1. The purple dots depict
1060 the low abundance proteins, orange dots depict the high abundance proteins and grey dots
1061 represent non-significant proteins. d-e) The heat maps depict the differential protein
1062 abundances in *Rv-vc*$_{dc}$+ATc, *Rv-secA1*$_{dc}$+ATc (d) and *Rv-vc*$_{dc}$+ATc, *Rv-tatA*$_{dc}$+ATc (e) using
1063 padj<0.05. The blue colour indicates the high abundant proteins and the orange colour
1064 represents the low abundance proteins. f) The Alluvial plots represent the number of proteins
1065 containing various signal peptides and their abundances upon SecA1 and TatAC depletion.

1066 **Figure 6: Membrane proteome of SecA1 and TatAC depleted cells.**

1067 a) Schematic diagram of membrane proteome data analysis of SecA1 and TatAC. Raw data
1068 was analysed using Uniprot database. The data was screened for spectral annotation and
1069 quantification. The transmembrane proteins were selected using DeepTMHMM 1.0 and
1070 Phobius. Localization of the proteins were also checked using psortb v3.0.3. The filtered
1071 proteins were normalised and differential protein abundances were plotted. Created in
1072 BioRender. Nandicoori, V. (2025) https://BioRender.com/u4nhpba. b-c) The volcano plots
1073 represent the proteins of SecA1 and TatAC depletion using padj<0.05 and $1 \geq \log_2$Fold
1074 Change≤ -1. The purple dots depict the low abundance proteins, orange dots depict the high

1075 abundance proteins and grey dots represent non-significant proteins. d-e) The heat maps
1076 depict the differential protein abundances in *Rv-vc*$_{dc}$+ATc, *Rv-secA1*$_{dc}$+ATc (d) and *Rv-*
1077 *vc*$_{dc}$+ATc, *Rv-tatA*$_{dc}$+ATc (e) membrane proteins. The blue colour depicts the high abundant
1078 proteins and the orange colour represents the low abundance proteins. f) The chord plot
1079 depicts the abundances of high and low proteins upon SecA1 depleted condition according
1080 to the different functional categories. g) The chord plot depicts the abundances of high and
1081 low proteins upon TatAC depleted condition according to the different functional categories.
1082 **Figure 7: Alteration of the cellular morphology upon SecA1 and TatA depletion.**
1083 a) SEM images of *Rv-vc*$_{dc}$ +ATc, *Rv-secA1*$_{dc}$ -/+ATc, *Rv-secA1*$_{dc}$*::secA1* +ATc, *Rv-tatA*$_{dc}$ -/+ATc,
1084 and *Rv-tatA*$_{dc}$*::tatAC* +ATc. *Rv-vc*$_{dc}$ +ATc, *Rv-secA1*$_{dc}$ -/+ATc, *Rv-secA1*$_{dc}$*::secA1* +ATc, *Rv-*
1085 *tatA*$_{dc}$ -/+ATc, *and Rv-tatA*$_{dc}$*::tatAC* +ATc were grown for 4 days post ATc addition, cells were
1086 fixed and processed for SEM. The images of cell morphology were taken through SEM at
1087 10,000x magnification. Scale bar 2 µm. b) Cell length (µm) for both SecA1 and TatAC was
1088 measured, quantified using ImageJ software and plotted using GraphPad Prism software. The
1089 statistical analysis was performed by One way ANOVA, **** $p<0.0001$. c) TEM images of *Rv-*
1090 *vc*$_{dc}$ +ATc, *Rv-secA1*$_{dc}$ -/+ATc, *Rv-secA1*$_{dc}$*::secA1* +ATc, *Rv-tatA*$_{dc}$ -/+ATc, *and Rv-tatA*$_{dc}$*::tatAC*
1091 +ATc. *Rv-vc*$_{dc}$ +ATc, *Rv-secA1*$_{dc}$ -/+ATc, *Rv-secA1*$_{dc}$*::secA1* +ATc, *Rv-tatA*$_{dc}$ -/+ATc, *and Rv-*
1092 *tatA*$_{dc}$*::tatAC* +ATc were grown for 4 days post ATc addition, cells were fixed and processed
1093 for TEM. The images of cell membrane were taken at 45,000x magnification. Scale bar 200
1094 nm. d) *Rv-vc*$_{dc}$ +ATc, *Rv-secA1*$_{dc}$ -/+ATc, *Rv-secA1*$_{dc}$*::secA1* +ATc, *Rv-tatA*$_{dc}$ -/+ATc, *and Rv-*
1095 *tatA*$_{dc}$*::tatAC* +ATc were grown and cells were harvested for the assays on day 2 and day 4
1096 post ATc treatment. A_{600} ~0.5 cells were treated with 5 µg/ml PI (Propidium Iodide), incubated
1097 for 30 min in dark and washed. The cells were fixed using 4% paraformaldehyde and PI
1098 positive cell populations were measured using flow cytometry. Excitation peak at 535 nm and
1099 emission peak at 617 nm. The shift in the fluorescence reading is shown here.
1100

1101 **Supplementary Figure S1: Schematic Representation of protein export through SecA1**
1102 **dependent Sec pathway and Tat pathway.**
1103 Pictorial model depicting the steps involved in SecA1 dependent secretion and TAT pathway
1104 when a protein contains: (a,d) N-terminal Sec/RR-motif signal sequence, Lipo motif and
1105 Transmembrane domain, (b,e) N-terminal Sec/RR-motif signal sequence and Lipo motif. (c,f)
1106 N-terminal Sec/RR-motif signal sequence and Transmembrane domain. The steps shown
1107 were based on the mechanistic reactions framed using the experimental evidence provided
1108 in Table S2. Created in BioRender. Nandicoori, V. (2025) https://BioRender.com/fy6pdxr.
1109 **Supplementary Figure S2: Schematic Representation of protein export through SRP**
1110 **dependent Sec pathway.**
1111 Pictorial model depicting the steps involved in SRP dependent secretion when a protein
1112 contains: (a) N-terminal SRP signal sequence, Lipo motif and Transmembrane domain, (b) N-
1113 terminal SRP signal sequence and Lipo motif, (c) N-terminal SRP signal sequence and
1114 Transmembrane domain, and (d) only N-terminal SRP signal sequence. The steps shown were
1115 based on the mechanistic reactions framed using the experimental evidence provided in Table
1116 S2. Created in BioRender. Nandicoori, V. (2025) https://BioRender.com/6e4dlep.
1117 **Supplementary Figure S3: CRISPRi mediated depletion strains of SecA1 and TatAC.**
1118 a) The vector maps represent here are of pTetInt-dCas9 vector for both SecA1 and TatA. b)
1119 The image shows the length of *secA1* (2850 bp) and *tatA* (252 bp) having the PAM sequences
1120 and guide RNAs binding regions. The yellow bars represent the PAM sequences and the red
1121 bars represent the respective guide RNA s for SecA1 and TatA. c) Schematic representation
1122 of CRISPRi mediated transcription inhibition upon addition of ATc. Created in BioRender.
1123 Nandicoori, V. (2025) https://BioRender.com/n0g7fiw. d) Diagram depicts the mechanism of
1124 complementation strains having guide RNA mutations in both *secA1* (*secA1*$_{gmut-1/2}$) and *tatA*
1125 (*tatA*$_{gmut1/2}$). e) Whole cell lysates (WCLs) were prepared from *Rv-vc*$_{dc}$+ATc, *Rv-secA1*$_{dc}$-/+ATc,
1126 *Rv-secA1*$_{dc}$*::secA1* +ATc, *Rv-tatA*$_{dc}$-/+ATc and *Rv-tatA*$_{dc}$*::tatAC* +ATc from grown 4th day
1127 culture. 50 µg of each protein lysates were resolved on 10% (SecA1) 15% (TatA) SDS-PAGE,
1128 transferred on Nitrocellulose membrane and probed with α-SecA1 (for SecA1 depletion), and

1129 α-TatA (for TatA depletion) antibodies generated in the lab. α-GroEL1 antibody was used as
1130 loading control.

1131 **Supplementary Figure S4: Isolation and validation of CF proteins from SecA1 and TatAC.**

1132 a) Schematic diagram of CF protein isolation from *Mtb Rv-vc*$_{dc}$, *Rv-secA1*$_{dc}$, and *Rv-tatA*$_{dc}$ cells
1133 in the presence of ATc. Created in BioRender. Nandicoori, V. (2025)
1134 https://BioRender.com/fauewmb. b) 50 µg of the isolated CFs fractions and WCL were
1135 resolved on SDS-PAGE, proteins were transferred onto Nitrocellulose membrane and probed
1136 with α-PknB (cytosolic protein), α-GroEL1 (cytosolic protein) and α-Ag85B (CF protein).
1137 Coomassie was performed as protein loading control. c) Venn diagram represents the
1138 comparison of our secretome data with four other studies performed by other groups
1139 available in the literature. d) The table represent the list of unique proteins identified in the
1140 secretome of *Rv-secA1*$_{dc}$+ATc and *Rv-tatA*$_{dc}$+ATc. The proteins highlighted in the green box
1141 represent the high abundant proteins and proteins highlighted in the red box represented
1142 the low abundant proteins. e) The table represent the list of common proteins identified in
1143 the secretome of *Rv-secA1*$_{dc}$+ATc and *Rv-tatA*$_{dc}$+ATc. The proteins highlighted in the green
1144 box represent the high abundant proteins and proteins highlighted in the red box
1145 represented the low abundant proteins.

1146 **Supplementary Figure S5: Validation of membrane proteome of SecA1 and TatAC membrane**
1147 **fractions.**

1148 a) Schematic representation of isolation of membrane and cytosolic fractions from *Rv-vc*$_{dc}$,
1149 *Rv-secA1*$_{dc}$, and *Rv-tatA*$_{dc}$ in presence of ATc. Created in BioRender. Nandicoori, V. (2025)
1150 https://BioRender.com/a0uooni. b) 50 µg of the isolated membrane, cytosol and WCL
1151 fractions were resolved on SDS-PAGE, proteins were transferred in the Nitrocellulose
1152 membrane and probed with α-PknB (membrane protein) and α-RpoA (cytosolic protein). c)
1153 The table represent the list of unique proteins identified in the membrane proteome of *Rv-*
1154 *secA1*$_{dc}$+ATc and *Rv-tatA*$_{dc}$+ATc. The proteins highlighted in the green box represent the high
1155 abundant proteins and proteins highlighted in the red box represented the low abundant
1156 proteins. e) The table represent the list of common proteins identified in the membrane
1157 proteome of *Rv-secA1*$_{dc}$+ATc and *Rv-tatA*$_{dc}$+ATc. The proteins highlighted in the green box

1158 represent the high abundant proteins and proteins highlighted in the red box represented
1159 the low abundant proteins.

1160 **Supplementary Figure S6: Validation of membrane alteration upon SecA1 and TatAC**
1161 **depletion.**

1162 a) The bars represent the % of cells having a cell length of <3 μm, 3-4 μm and >4 μm in *Rv-*
1163 *vc_{dc}* +ATc, *Rv-secA1$_{dc}$* -/+ATc, *Rv-secA1$_{dc}$::secA1* +ATc, *Rv-tatA$_{dc}$* -/+ATc and *Rv-tatA$_{dc}$::tatA*
1164 +ATc. b) The bars depict the percentage of bulged cells vs normal cells in *Rv-vc_{dc}* +ATc, *Rv-*
1165 *secA1$_{dc}$* -/+ATc, *Rv-secA1$_{dc}$::secA1* +ATc. c) The graphs represent the fluorescence (A.U.) upon
1166 EtBr uptake by *Rv-vc_{dc}* +ATc, *Rv-secA1$_{dc}$* -/+ATc, *Rv-secA1$_{dc}$::secA1* +ATc strains on Day 2 and
1167 Day 4. d) The graphs represent the fluorescence (A.U.) upon EtBr uptake by *Rv-vc_{dc}* +ATc, *Rv-*
1168 *tatA$_{dc}$* -/+ATc, *Rv-tatA$_{dc}$::tatA* +ATc strains on Day 2 and Day 4.

1169

Figure 1.

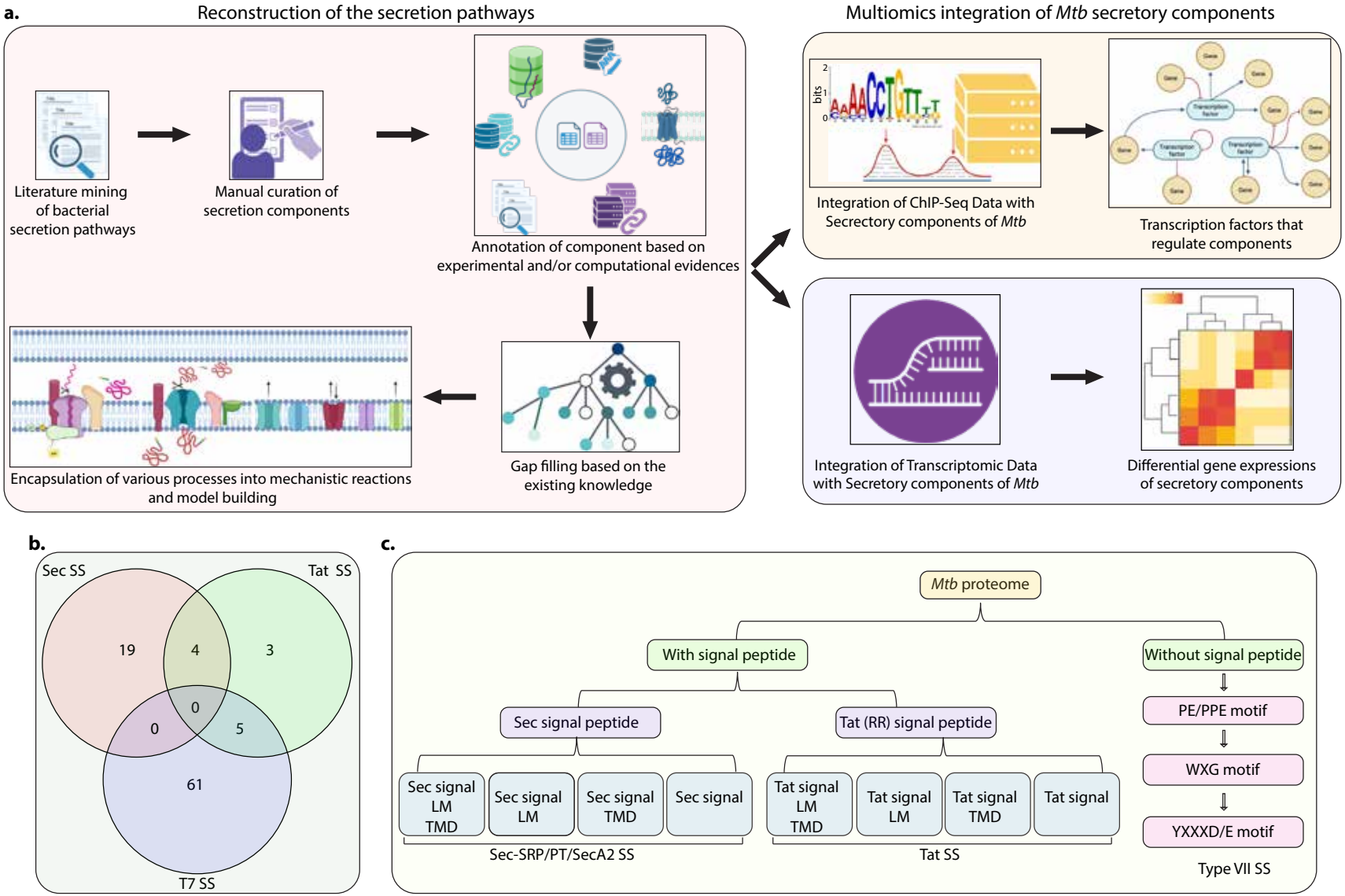
a.
Reconstruction of the secretion pathways
Literature mining of bacterial secretion pathways
Manual curation of secretion components
Annotation of component based on experimental and/or computational evidences
Gap filling based on the existing knowledge
Encapsulation of various processes into mechanistic reactions and model building
Multiomics integration of Mtb secretory components
Integration of ChIP-Seq Data with Secretory components of Mtb
Transcription factors that regulate components
Integration of Transcriptomic Data with Secretory components of Mtb
Differential gene expressions of secretory components
b.
Sec SS
Tat SS
19
4
3
0
0
5
61
T7 SS
c.
Mtb proteome
With signal peptide
Without signal peptide
Sec signal peptide
Tat (RR) signal peptide
Sec signal LM TMD
Sec signal LM
Sec signal TMD
Sec signal
Tat signal LM TMD
Tat signal LM
Tat signal TMD
Tat signal
Sec-SRP/PT/SecA2 SS
Tat SS
PE/PPE motif
WXG motif
YXXXD/E motif
Type VII SS

Figure 2.

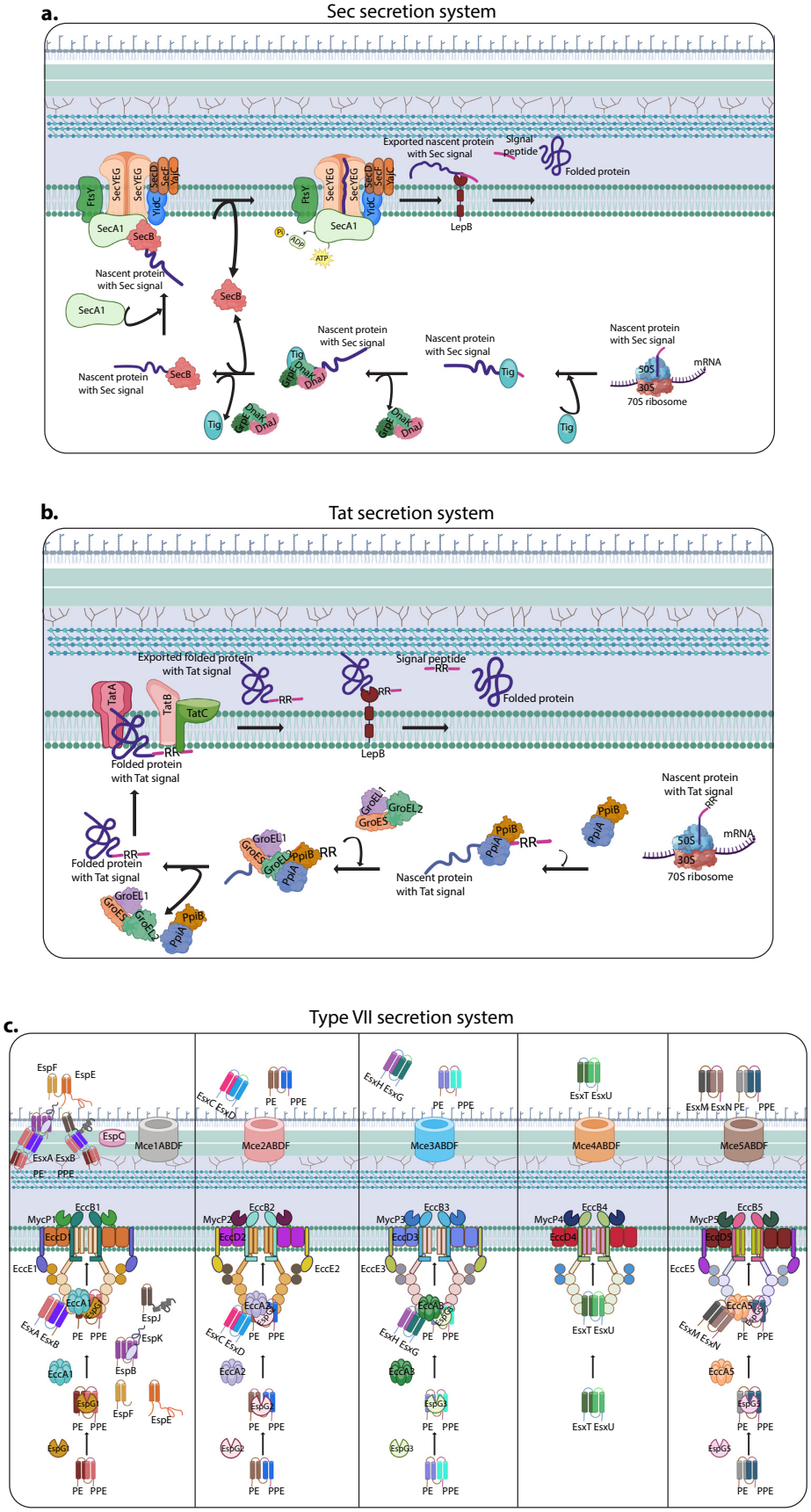
a.
Sec secretion system
Exported nascent protein with Sec signal
Signal peptide
Folded protein
FtsY
SecYEG
SecD
SecF
YajC
YidC
SecA1
SecB
LepB
Pi
ADP
ATP
Nascent protein with Sec signal
Tig
DnaK
DnaJ
mRNA
50S
30S
70S ribosome
b.
Tat secretion system
Exported folded protein with Tat signal
Signal peptide
RR
TatA
TatB
TatC
Folded protein
LepB
Folded protein with Tat signal
Nascent protein with Tat signal
GroEL1
GroEL2
GroES
PpiA
PpiB
mRNA
50S
30S
70S ribosome
c.
Type VII secretion system
EspF
EspE
EspC
Mce1ABDF
Mce2ABDF
Mce3ABDF
Mce4ABDF
Mce5ABDF
EsxA EsxB
EsxC EsxD
EsxH EsxG
EsxT EsxU
EsxM EsxN
PE
PPE
MycP1
MycP2
MycP3
MycP4
MycP5
EccB1
EccB2
EccB3
EccB4
EccB5
EccD1
EccD2
EccD3
EccD4
EccD5
EccE1
EccE2
EccE3
EccE5
EccA1
EccA2
EccA3
EccA5
EspG1
EspG2
EspG3
EspG5
EspJ
EspK
EspB

Figure 3.

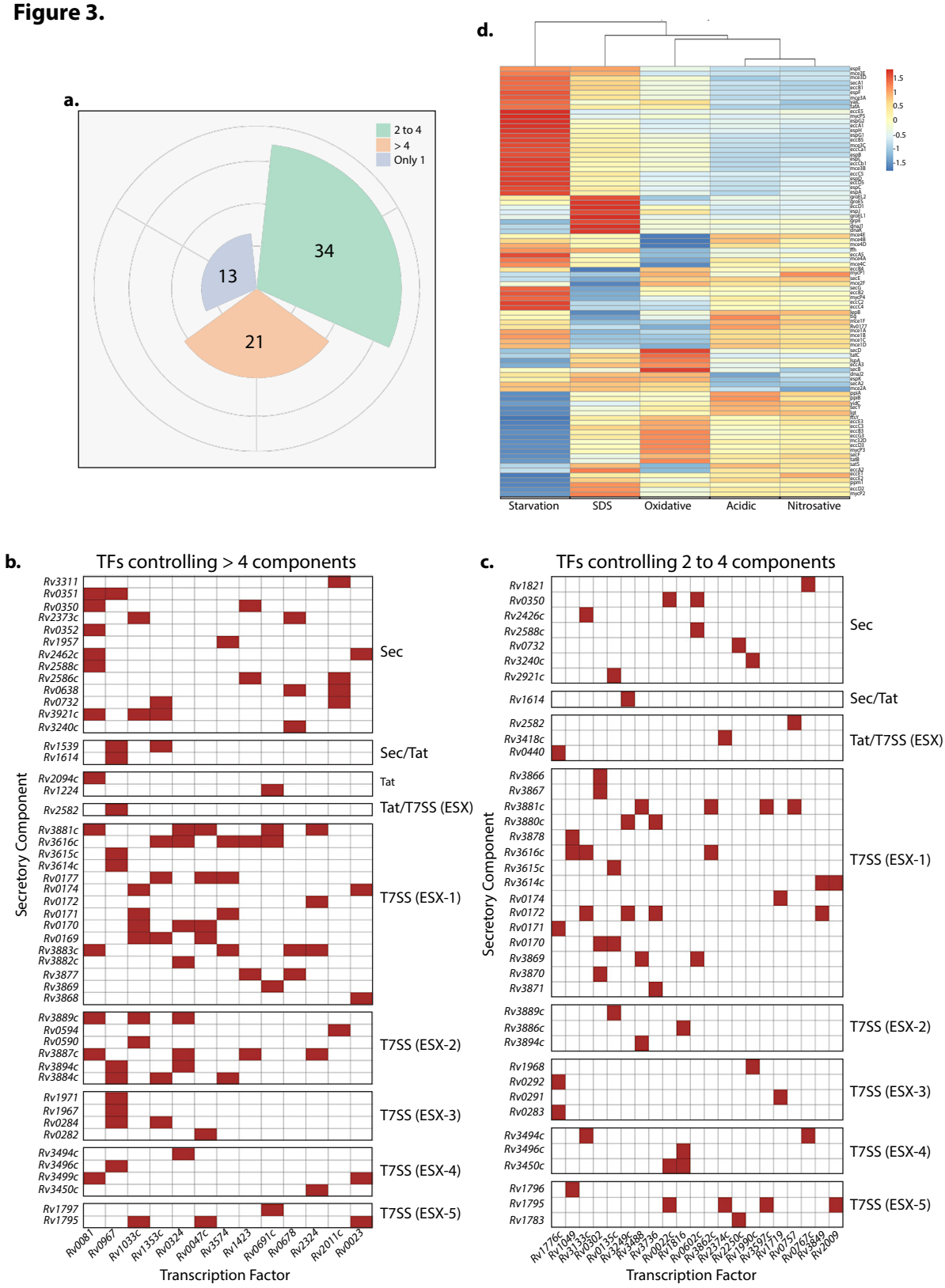
a.
2 to 4
> 4
Only 1
34
21
13
d.
Starvation
SDS
Oxidative
Acidic
Nitrosative
b.
TFs controlling > 4 components
Secretory Component
Sec
Sec/Tat
Tat
Tat/T7SS (ESX)
T7SS (ESX-1)
T7SS (ESX-2)
T7SS (ESX-3)
T7SS (ESX-4)
T7SS (ESX-5)
Transcription Factor
c.
TFs controlling 2 to 4 components
Secretory Component
Sec
Sec/Tat
Tat/T7SS (ESX)
T7SS (ESX-1)
T7SS (ESX-2)
T7SS (ESX-3)
T7SS (ESX-4)
T7SS (ESX-5)
Transcription Factor

Figure 4.

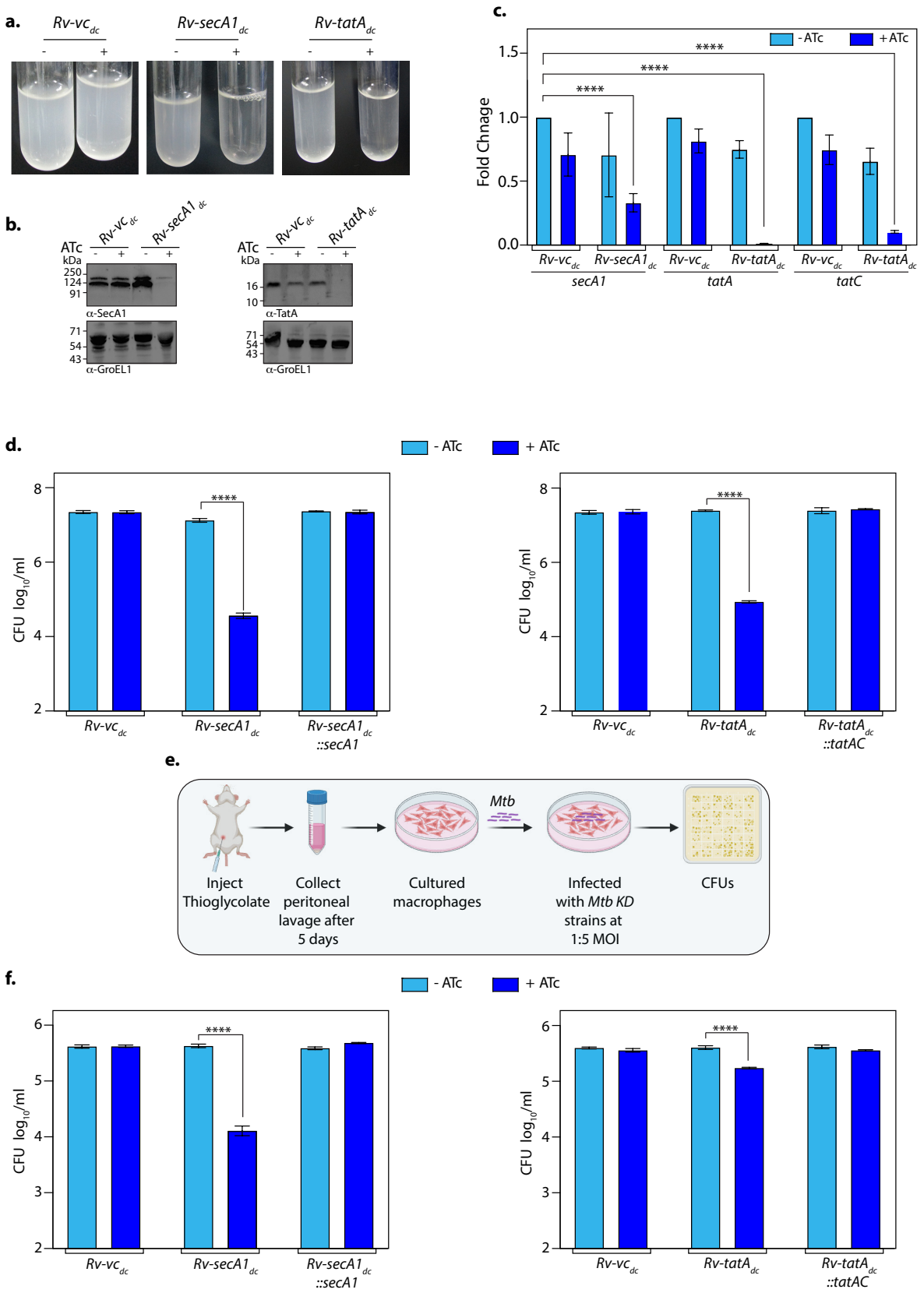
a.
Rv-vc dc
Rv-secA1 dc
Rv-tatA dc
- +
b.
ATc
kDa
250
124
91
α-SecA1
71
54
43
α-GroEL1
16
10
α-TatA
c.
- ATc
+ ATc
Fold Chnage
1.5
1.0
0.5
0.0
****
Rv-vc dc
Rv-secA1 dc
Rv-tatA dc
secA1
tatA
tatC
d.
CFU log10/ml
8
6
4
2
Rv-secA1 dc ::secA1
Rv-tatA dc ::tatAC
e.
Mtb
Inject Thioglycolate
Collect peritoneal lavage after 5 days
Cultured macrophages
Infected with Mtb KD strains at 1:5 MOI
CFUs
f.
5
3

Figure 5.

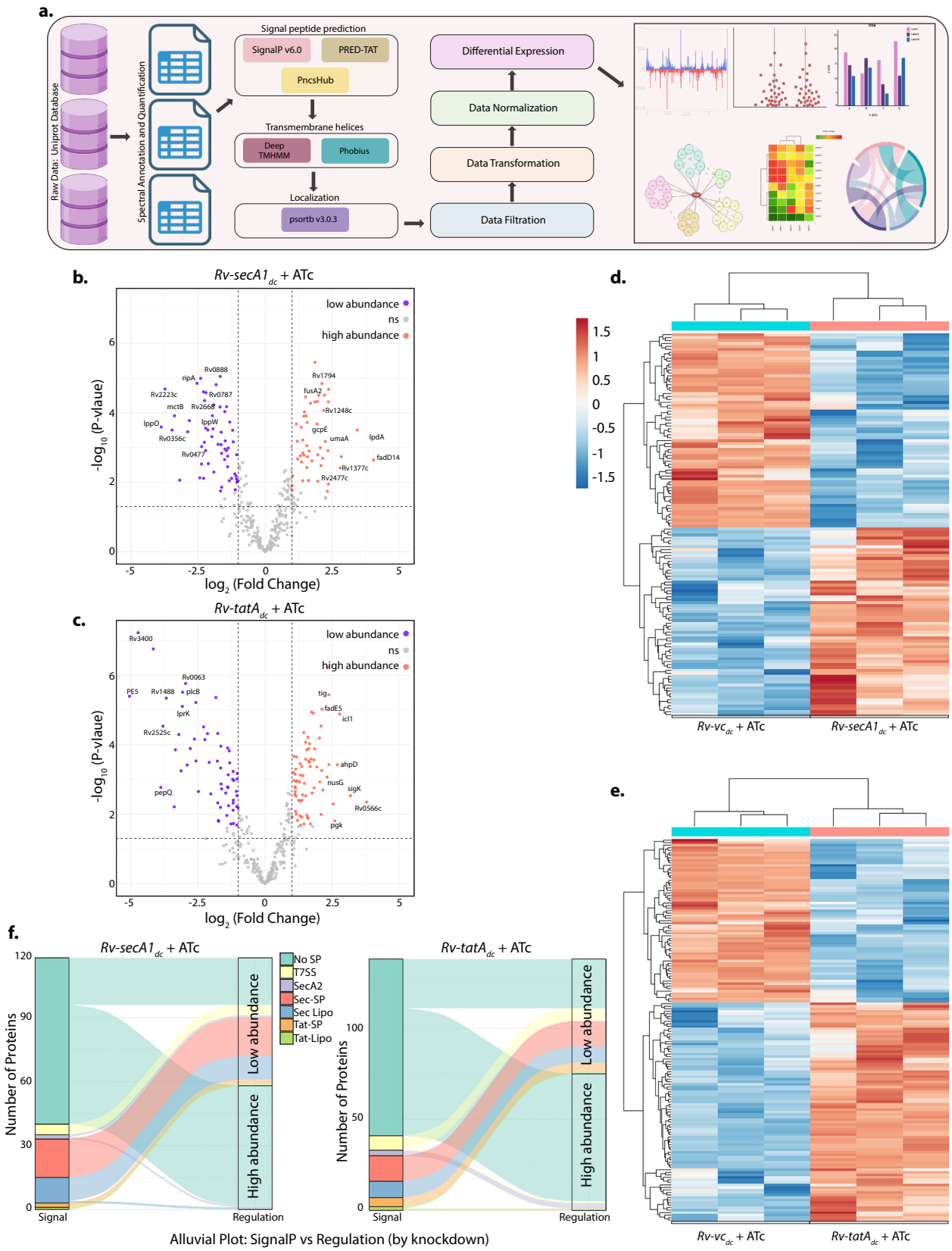
a.
Raw Data: Uniprot Database
Spectral Annotation and Quantification
Signal peptide prediction
SignalP v6.0
PRED-TAT
PncsHub
Transmembrane helices
Deep TMHMM
Phobius
Localization
psortb v3.0.3
Differential Expression
Data Normalization
Data Transformation
Data Filtration
b.
Rv-secA1dc + ATc
low abundance
ns
high abundance
-log10 (P-vlaue)
log2 (Fold Change)
c.
Rv-tatAdc + ATc
d.
Rv-vcdc + ATc
Rv-secA1dc + ATc
e.
Rv-vcdc + ATc
Rv-tatAdc + ATc
f.
Rv-secA1dc + ATc
Rv-tatAdc + ATc
Number of Proteins
Signal
Regulation
Low abundance
High abundance
No SP
T7SS
SecA2
Sec-SP
Sec Lipo
Tat-SP
Tat-Lipo
Alluvial Plot: SignalP vs Regulation (by knockdown)

Figure 6.

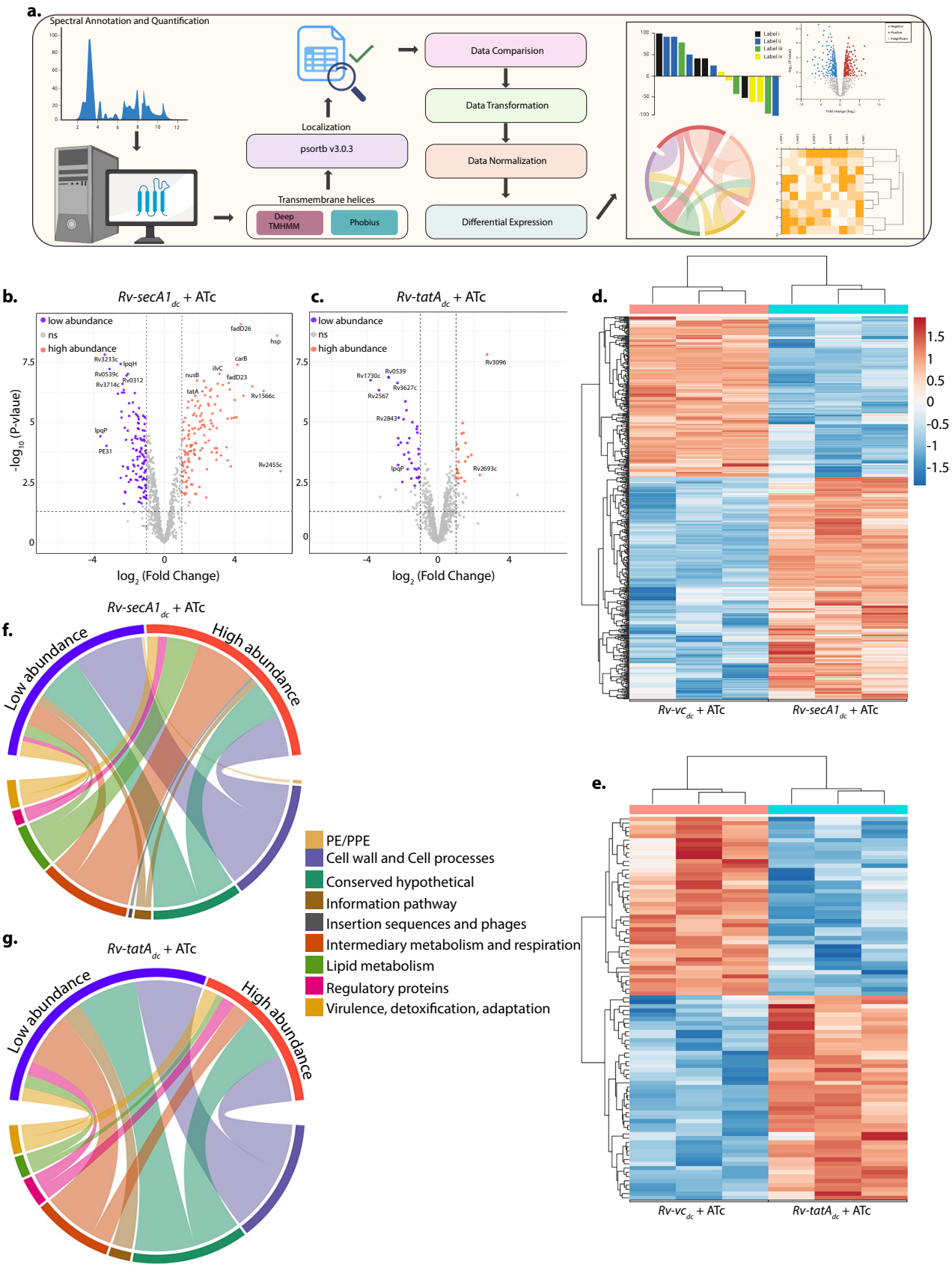
a.
Spectral Annotation and Quantification
Localization
psortb v3.0.3
Transmembrane helices
Deep TMHMM
Phobius
Data Comparision
Data Transformation
Data Normalization
Differential Expression
b.
Rv-secA1dc + ATc
low abundance
ns
high abundance
-log10 (P-vlaue)
log2 (Fold Change)
c.
Rv-tatAdc + ATc
d.
Rv-vcdc + ATc
Rv-secA1dc + ATc
e.
Rv-vcdc + ATc
Rv-tatAdc + ATc
f.
Rv-secA1dc + ATc
Low abundance
High abundance
g.
Rv-tatAdc + ATc
PE/PPE
Cell wall and Cell processes
Conserved hypothetical
Information pathway
Insertion sequences and phages
Intermediary metabolism and respiration
Lipid metabolism
Regulatory proteins
Virulence, detoxification, adaptation

Figure 7.

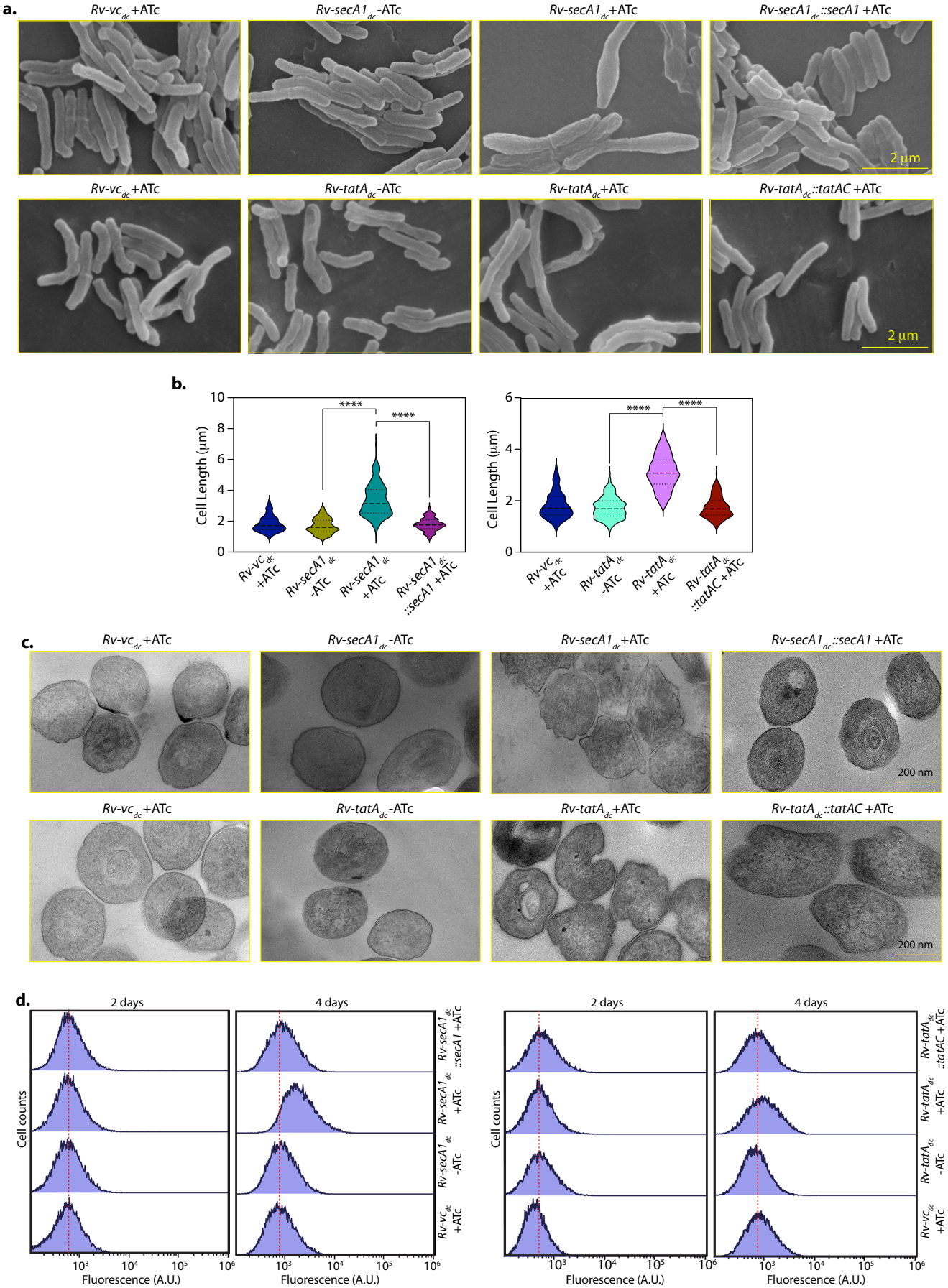
a.
Rv-vc$_{dc}$+ATc
Rv-secA1$_{dc}$-ATc
Rv-secA1$_{dc}$+ATc
Rv-secA1$_{dc}$::secA1 +ATc
2 µm
Rv-vc$_{dc}$+ATc
Rv-tatA$_{dc}$-ATc
Rv-tatA$_{dc}$+ATc
Rv-tatA$_{dc}$::tatAC +ATc
2 µm
b.
Cell Length (µm)
****
****
Rv-vc$_{dc}$ +ATc
Rv-secA1$_{dc}$ -ATc
Rv-secA1$_{dc}$ +ATc
Rv-secA1$_{dc}$ ::secA1 +ATc
Cell Length (µm)
****
****
Rv-vc$_{dc}$ +ATc
Rv-tatA$_{dc}$ -ATc
Rv-tatA$_{dc}$ +ATc
Rv-tatA$_{dc}$ ::tatAC +ATc
c.
Rv-vc$_{dc}$+ATc
Rv-secA1$_{dc}$-ATc
Rv-secA1$_{dc}$+ATc
Rv-secA1$_{dc}$::secA1 +ATc
200 nm
Rv-vc$_{dc}$+ATc
Rv-tatA$_{dc}$-ATc
Rv-tatA$_{dc}$+ATc
Rv-tatA$_{dc}$::tatAC +ATc
200 nm
d.
2 days
4 days
Cell counts
Rv-secA1$_{dc}$ ::secA1 +ATc
Rv-secA1$_{dc}$ +ATc
Rv-secA1$_{dc}$ -ATc
Rv-vc$_{dc}$ +ATc
Fluorescence (A.U.)
Fluorescence (A.U.)
2 days
4 days
Cell counts
Rv-tatA$_{dc}$ ::tatAC +ATc
Rv-tatA$_{dc}$ +ATc
Rv-tatA$_{dc}$ -ATc
Rv-vc$_{dc}$ +ATc
Fluorescence (A.U.)
Fluorescence (A.U.)